

**A stabilized total pressure-formulation of the Biot's poroelasticity  
equations in frequency domain: numerical analysis and  
applications**

Cristian Cárcamo<sup>1</sup>, Alfonso Caiazzo<sup>1</sup>, Felipe Galarce<sup>2</sup>, Joaquín Mura<sup>3</sup>

submitted: April 17, 2024

<sup>1</sup> Weierstrass Institute

Mohrenstr. 39

10117 Berlin, Germany

E-Mail: cristian.carcamosanchez@wias-berlin.de

alfonso.caiazzo@wias-berlin.de

<sup>2</sup> School of Civil Engineering

Pontificia Universidad Católica de Valparaíso

Valparaíso, Chile

E-Mail: felipe.galarce@pucv.cl

<sup>3</sup> Department of Mechanical Engineering

Universidad Técnica Federico Santa María

Santiago, Chile

E-Mail: joaquin.mura@usm.cl

No. 3101

Berlin 2024



Edited by  
Weierstraß-Institut für Angewandte Analysis und Stochastik (WIAS)  
Leibniz-Institut im Forschungsverbund Berlin e. V.  
Mohrenstraße 39  
10117 Berlin  
Germany

Fax: +49 30 20372-303  
E-Mail: [preprint@wias-berlin.de](mailto:preprint@wias-berlin.de)  
World Wide Web: <http://www.wias-berlin.de/>

# A stabilized total pressure-formulation of the Biot's poroelasticity equations in frequency domain: numerical analysis and applications

Cristian Cárcamo, Alfonso Caiazzo, Felipe Galarce, Joaquín Mura

## Abstract

This work focuses on the numerical solution of the dynamics of a poroelastic material in the frequency domain. We provide a detailed stability analysis based on the application of the Fredholm alternative in the continuous case, considering a total pressure formulation of the Biot's equations. In the discrete setting, we propose a stabilized equal order finite element method complemented by an additional pressure stabilization to enhance the robustness of the numerical scheme with respect to the fluid permeability. Utilizing the Fredholm alternative, we extend the well-posedness results to the discrete setting, obtaining theoretical optimal convergence for the case of linear finite elements. We present different numerical experiments to validate the proposed method. First, we consider model problems with known analytic solutions in two and three dimensions. As next, we show that the method is robust for a wide range of permeabilities, including the case of discontinuous coefficients. Lastly, we show the application for the simulation of brain elastography on a realistic brain geometry obtained from medical imaging.

## 1 Introduction

This paper focuses on the simulation of poroelastic materials following Biot's equations [5], in which the interplay of bulk deformation, fluid flow, and fluid pressure is modeled coupling linear elasticity with a flow through a deformable porous media. This model has been widely applied in diverse fields ranging from hydrology and geomechanics (see, e.g., [43]) to biomechanics [37]), and fluid transport in soft tissue such as perfusion [41, 36]

Our work is motivated by the application of poroelastic modeling for the solution of inverse problems in tissue imaging, in particular in Magnetic Resonance Elastography (MRE) (see, e.g., [21, 34]), an acquisition technique which is sensitive to tissue motion. In MRE, the tissue undergoes a harmonic excitation at given frequencies, while the tissue displacement field is reconstructed via phase-contrast MRI. Combining the reconstructed displacement with a physical tissue model allows hence to estimate relevant biomechanical parameters. Recent applications of poroelastic tissue models in the context of inverse problems in MRE can be found, e.g., in [29, 39].

From the perspective of numerical analysis, there are several works focusing on suitable numerical methods for poroelastic materials, including standard Galerkin method [27], adaptive algorithms [22], mixed variational formulations through the introduction of a Lagrange multiplier and related [1, 24, 42], Discontinuous Galerkin [30], adaptive strategies (also for multiple-network poroelasticity equations) [13, 25, 33], highlighting also new methods facilitating the use of general meshes such as Hybrid High Order (HHO) method [6] or Virtual Element Method (VEM) [9]. Additionally, in [4], an overview of the Theory of Porous Media restricted to small deformations and its discretization is provided.

We propose and analyze a numerical scheme in the frequency domain based on equal-order finite elements, a choice which allows to maintain low the computational cost also in three dimensions. The scheme use a displacement-pressure-total pressure formulation, equipped with a residual-based stabilization term, inspired by the work of [28] in the static setting, which ensures stability between the space of displacements and the space of total pressures.

The main contribution of this work concerns the detailed numerical analysis, in the continuous and in the discrete settings. Using the Fredholm alternative, we extend the results of [28] to the frequency domain, showing that the total pressure formulation is stable under the assumption of stability of the underlying elastic problem. In particular, we show that the operator defining the differential problem can be written as a compact perturbation of a bijective one (see, e.g., [15, 32, 23]).

One of the most difficult scenarios to deal with is the case of low permeability regions. In those situations, so-called poroelastic locking might result in nonphysical fast pressure oscillations, which can be cured using particular finite element spaces [31, 28]. In the context of inverse problems, where the parameters are unknown a priori, it is therefore of utmost importance to consider a numerical method that can robustly handle the appearance of low permeability regions throughout the domain. To this purpose, we propose an additional pressure stabilization, which introduces an additional control on the pressure gradient. The stabilization term, inspired by a Brezzi-Pitkäranta stabilization [8] acts as an artificial local permeability when the physical permeability becomes too low.

We benchmark the proposed method in several numerical tests, validating the expected convergence orders, as well as the robustness of the formulation for low permeabilities.

The rest of the paper is organized as follows. Section 2 introduces the model problem. The analysis in the continuous case is presented in Section 3, while Section 4 discusses the proposed numerical method and the extension of the well-posedness analysis in the case of the considered stabilized finite element formulation. The numerical results are presented in Section 5, while Section 6 draws the conclusions.

## 2 Model Problem

### 2.1 Linear poroelasticity in the harmonic regime

Poroelasticity describes the coupled motion of solid matrix deformation and fluid flow in a porous medium. The equations governing the dynamics consist of a balance of linear momentum for the solid phase, a mass conservation equation for the fluid phase, and a constitutive relation that relates the stress and strain in the solid phase to the fluid pressure.

Following Biot's theory (see, e.g., [5, 35, 26]), we consider the motion of a poroelastic medium in a sufficiently regular computational domain  $\Omega \subset \mathbb{R}^d$ . The medium is described by a displacement field  $\mathbf{u} : \Omega \rightarrow \mathbb{R}^d$  and a pressure field  $p : \Omega \rightarrow \mathbb{R}$  both serving as solutions to:

$$\begin{cases} \rho \mathbf{u}_{tt} - \operatorname{div} \boldsymbol{\sigma} + \nabla p = \mathbf{0} & \text{in } \Omega \times [0, T] \\ S_\epsilon p_t + \alpha \operatorname{div} \mathbf{u}_t - \frac{\kappa}{\mu_f} \Delta p = 0 & \text{in } \Omega \times [0, T] \end{cases} \quad (1)$$

In (1), the symbol  $\boldsymbol{\sigma}$  represents the Cauchy solid stress, defined as

$$\boldsymbol{\sigma} := 2\mu_e \boldsymbol{\varepsilon}(\mathbf{u}) + \lambda(\nabla \cdot \mathbf{u})\mathbb{I}, \quad (2)$$

where  $\varepsilon(\mathbf{u})$  is the infinitesimal strain tensor,  $\mathbb{I}$  represents the identity tensor, and the Lamé coefficients are given by

$$\mu_e := \frac{E}{2(1+\nu)}, \quad \lambda := \frac{E\nu}{(1+\nu)(1-2\nu)},$$

as functions of the Young modulus  $E$  and of the Poisson ratio  $\nu$ .

The parameter  $\kappa$  in (1) represents the permeability of the porous medium, while  $\mu_f, \rho > 0$  denote the fluid viscosity and density, respectively. Additionally,  $\alpha > 0$  is the Biot-Willis parameter,  $B$  is the so-called Skempton's parameter, and the mass storage parameter  $S_\epsilon$  is defined as

$$S_\epsilon = 3\alpha(1 - \alpha B)(1 - 2\nu)(BE)^{-1}.$$

Following the approach of [28], we then introduce the *total pressure*

$$\phi = p - \lambda \operatorname{tr}(\varepsilon(\mathbf{u})). \quad (3)$$

This work is motivated by applications in which the material undergoes harmonic excitation at a given frequency (see, e.g., the case of elastic tissue imaging such as MRE [16, 21]). We hence focus on system (1) in the harmonic regime for a single *given* frequency  $\omega$ :

$$\begin{cases} -\omega^2 \rho \mathbf{u} - \operatorname{div}(2\mu_e \varepsilon(\mathbf{u}) - \phi \mathbb{I}) = \mathbf{0} \\ i \left( S_\epsilon + \frac{\alpha}{\lambda} \right) \omega p - i\omega \frac{\alpha}{\lambda} \phi - \frac{\kappa}{\mu_f} \Delta p = 0, \\ \phi - p + \lambda \operatorname{tr}(\varepsilon(\mathbf{u})) = 0. \end{cases} \quad (4)$$

With a slight abuse of notation, we will denote the (complex-valued)  $\omega$ -Fourier modes of velocity, pressure, and total pressure as  $\mathbf{u}$ ,  $p$ , and  $\phi$ , respectively, while  $i$  represents the imaginary unit.

Moreover, we introduce the (dimensionless) parameter

$$\theta := \frac{S_\epsilon \lambda}{\alpha} + 1 = \frac{3\nu\alpha(1 - \alpha B)}{\alpha B(1 + \nu)(1 - 2\nu)^2} + 1. \quad (5)$$

The system (4) shall be complemented by appropriate boundary conditions on the displacement and pressure fields. Throughout the rest of this work, we assume that the boundary of the domain is decomposed as

$$\partial\Omega = \Gamma_u \cup \Gamma_p.$$

Denoting  $\mathbf{n}$  as the outward normal vector to the boundary, we consider boundary conditions of the form

$$\begin{cases} \mathbf{u} = \mathbf{0} & \text{on } \Gamma_u \\ \sigma \mathbf{n} = \mathbf{g}^u & \text{on } \Gamma_p \end{cases} \quad (6)$$

for the displacement, and

$$\begin{cases} p = 0 & \text{on } \Gamma_p \\ \frac{\kappa}{\mu_f} \partial_{\mathbf{n}} p = g^p & \text{on } \Gamma_u \end{cases} \quad (7)$$

for the pressure.

## 2.2 Weak formulation

Let us consider the standard Sobolev spaces  $L^2(\Omega)$  and  $H^1(\Omega)$  of complex-valued functions equipped with the inner products

$$(u, v)_\Omega := (u, v)_{L^2(\Omega)} := \int_\Omega u \bar{v}, \quad (8)$$

and

$$(u, v)_{1,\Omega} := (u, v)_{H^1(\Omega)} = (u, v)_\Omega + \ell^2 \sum_{i=1}^d \left( \frac{\partial u}{\partial x_i}, \frac{\partial v}{\partial x_i} \right)_\Omega, \quad (9)$$

respectively, where  $\bar{v}$  stands for the complex conjugate of  $v$ . In (9), the parameter  $\ell$  denotes a typical length of the domain  $\Omega$ , and it has been introduced for the purpose of maintaining consistency in physical units.

Let us also denote with  $\|\cdot\|_0$  and  $\|\cdot\|_1$  the standard norms induced by the above inner products, and introduce the seminorm

$$|v|_1^2 := \sum_{i=1}^d \left\| \frac{\partial u}{\partial x_i} \right\|_\Omega^2,$$

such that  $\|v\|_1 = \|v\|_0 + \ell^2 |v|_1$ , for any  $v \in H^1(\Omega)$ .

For any subset in  $\Gamma \subset \partial\Omega$ , we also denote by  $L^2(\Gamma)$  the space of integrable functions on  $\Gamma$  and by  $\langle \cdot, \cdot \rangle_\Gamma$  the corresponding inner product.

In the above setting, let us introduce the functional spaces

$$\begin{aligned} \mathbf{H} &:= \{ \mathbf{v} : \Omega \rightarrow \mathbb{C}^d, \mathbf{v} \in H^1(\Omega)^d : \mathbf{v} = \mathbf{0} \text{ on } \Gamma_u \}, \\ P &:= \{ q : \Omega \rightarrow \mathbb{C}, q \in H^1(\Omega) : q = 0 \text{ on } \Gamma_p \} \\ S &:= L^2(\Omega), \end{aligned} \quad (10)$$

as well as the product space  $\mathbf{U} := \mathbf{H} \times P \times S$ , equipped with the norm

$$\|(\mathbf{v}, q, \xi)\|_{\mathbf{U}}^2 := 2\mu_e \|\varepsilon(\mathbf{v})\|_0^2 + \frac{\kappa}{\mu_f \omega \alpha} \|q\|_1^2 + \lambda^{-1} \|\xi\|_0^2. \quad (11)$$

As next, we introduce the bilinear forms

$$a_1 : \mathbf{H} \times \mathbf{H} \rightarrow \mathbb{C}, \quad a_1(\mathbf{u}, \mathbf{v}) := -\omega^2 \rho(\mathbf{u}, \mathbf{v}) + 2\mu_e (\varepsilon(\mathbf{u}), \varepsilon(\mathbf{v})) \quad (12)$$

$$a_2 : P \times P \rightarrow \mathbb{C}, \quad a_2(p, q) := i\theta \lambda^{-1} (p, q) + \frac{\kappa}{\mu_f \omega \alpha} (\nabla p, \nabla q) \quad (13)$$

$$\tilde{b} : \mathbf{H} \times S \rightarrow \mathbb{C}, \quad \tilde{b}(\mathbf{u}, \xi) := -(\operatorname{div} \mathbf{u}, \xi) \quad (14)$$

$$\tilde{b}^* : S \times \mathbf{H} \rightarrow \mathbb{C}, \quad \tilde{b}^*(\phi, \mathbf{v}) := -(\phi, \operatorname{div} \mathbf{v}) \quad (15)$$

$$c : P \times S \rightarrow \mathbb{C}, \quad c(p, \xi) := -\lambda^{-1} (p, \xi) \quad (16)$$

$$c^* : S \times P \rightarrow \mathbb{C}, \quad c^*(\phi, q) := -\lambda^{-1} (\phi, q) \quad (17)$$

$$d : S \times S \rightarrow \mathbb{C}, \quad d(\phi, \xi) := \lambda^{-1} (\phi, \xi). \quad (18)$$

Multiplying the equations of system (4) by  $\mathbf{v} \in \mathbf{H}$ ,  $q \in P$ , and  $\xi \in S$ , respectively, integrating by parts, and imposing the boundary conditions (6)-(7), we consider problem: Find  $\vec{\mathbf{u}} = (\mathbf{u}, p, \phi) \in \mathbf{U}$  such that

$$\langle \mathcal{A}(\vec{\mathbf{u}}), \vec{\mathbf{v}} \rangle = \langle \mathcal{F}, \vec{\mathbf{v}} \rangle \quad (19)$$

for all  $\vec{v} = (\mathbf{v}, q, \xi) \in \mathbf{U}$ , where  $\mathcal{A} : \mathbf{U} \rightarrow \mathbf{U}^*$  is defined by

$$\langle \mathcal{A}(\vec{\mathbf{u}}), \vec{\mathbf{v}} \rangle := a_1(\mathbf{u}, \mathbf{v}) + \tilde{b}^*(\phi, \mathbf{v}) + a_2(p, q) + ic^*(\phi, q) + d(\phi, \xi) + c(p, \xi) - \tilde{b}(\mathbf{u}, \xi), \quad (20)$$

and  $\mathcal{F} \in \mathbf{U}^*$  is defined by

$$\langle \mathcal{F}, \vec{\mathbf{v}} \rangle := \langle \mathbf{g}^u, \mathbf{v} \rangle_{\Gamma_p} + \frac{1}{\omega} \langle g^p, q \rangle_{\Gamma_u}. \quad (21)$$

We also introduce the operators  $\mathcal{B} : \mathbf{U} \rightarrow \mathbf{U}^*$  and  $\mathcal{C} : \mathbf{U} \rightarrow \mathbf{U}^*$  defined by

$$\langle \mathcal{B}(\vec{\mathbf{u}}), \vec{\mathbf{v}} \rangle := a_1(\mathbf{u}, \mathbf{v}) + \tilde{b}^*(\phi, \mathbf{v}) + a_2(p, q) + d(\phi, \xi) - \tilde{b}(\mathbf{u}, \xi), \quad (22)$$

and

$$\langle \mathcal{C}(\vec{\mathbf{u}}), \vec{\mathbf{v}} \rangle := ic^*(\phi, q) + c(p, \xi), \quad (23)$$

respectively. These operators allow us to rewrite

$$\mathcal{A} = \mathcal{B} + \mathcal{C}. \quad (24)$$

The decomposition (24) will be utilized to establish the well-posedness of the weak formulation (20)-(21) by employing Fredholm's alternative (see, e.g., [15]). The alternative states that an operator is bijective if it can be written as a sum of a bijective operator and a compact operator.

### 3 Analysis of the continuous problem

#### 3.1 Preliminaries

To begin with, let us recall a few essential theoretical results which will be required for the upcoming analysis.

**Theorem 1** (Poincaré inequality). *There exists a positive constant  $C_P$ , depending on  $\Omega$ , such that*

$$\|q\|_1 \leq C_P \ell^2 \|q\|_0, \quad (25)$$

for all  $q \in H^1(\Omega)$ .

*Proof.* See, e.g., [7]. □

**Theorem 2** (Trace inequality). *Assuming that  $\Omega$  has a Lipschitz boundary and  $p \in \mathbb{R}$  with  $1 \leq p \leq \infty$ , the following trace inequality holds: there exists a constant  $C > 0$  such that*

$$\|\mathbf{v}\|_{0,\Gamma} = \sqrt{\langle \mathbf{v}, \mathbf{v} \rangle_{\Gamma}} \leq C \|\mathbf{v}\|_0^{\frac{1}{2}} \|\mathbf{v}\|_1^{\frac{1}{2}}, \quad (26)$$

for all  $\mathbf{v} \in H^1(\Omega)^d$ .

*Proof.* See, e.g., [7]. □

**Theorem 3** (Korn inequality). *There exist a positive constant  $C_K$ , dependent on  $\Omega$ , such that*

$$\|\mathbf{v}\|_1 \leq C_K \|\varepsilon(\mathbf{v})\|_0, \quad (27)$$

holds for all  $\mathbf{v} \in H^1(\Omega)^d$ .

*Proof.* See, e.g., [11, Theorem 6.15-4]. □

For the following proofs, the following weaker definition of coercivity and is required.

**Definition 4** (*T-coercivity*). Let  $(V, \langle \cdot, \cdot \rangle_V)$  and  $(W, \langle \cdot, \cdot \rangle_W)$  be two Hilbert spaces. A linear operator  $L : V \rightarrow W^*$  is called *T-coercive* if there exists  $T \in \mathcal{L}(V, W)$  bijective and a constant  $\tilde{\alpha} > 0$ , such that

$$|\langle L(v), T(v) \rangle| \geq \tilde{\alpha} \|v\|_V^2,$$

holds for all  $v \in V$ .

As demonstrated in [10], the property of *T-coercive* is sufficient to establish the well-posedness of the corresponding bilinear form.

**Theorem 5.** Let  $L : V \rightarrow W^*$  be a linear operator, and let  $\langle L(u), v \rangle$  be the induced bilinear form over the product space  $V \times W$ . Then, the following statements are equivalent:

- i) The problem  $\langle L(u), v \rangle = \langle f, v \rangle$  is well-posed, for any  $f \in W$
- ii)  $L$  is *T-coercive*.

For the proof, we refer the reader to [10].

Finally, the following result will be used to show the well-posedness of the variational problem, exploiting the structure of the operators in the product space  $\mathbf{U} = \mathbf{H} \times P \times S$ .

**Theorem 6.** Let  $(V, \langle \cdot, \cdot \rangle_V)$  and  $(Z, \langle \cdot, \cdot \rangle_Z)$  be two Hilbert spaces and let us consider a linear operator  $\mathbb{T} : V \times Z \rightarrow V^* \times Z^*$  on the product space that can be written in the form

$$\mathbb{T}(v, z) = \begin{pmatrix} A & B^* \\ B & C \end{pmatrix} \begin{pmatrix} v \\ z \end{pmatrix} = (A(v) + B^*(z), B(v) + C(z)) \quad (28)$$

for bounded linear operators  $A : V \rightarrow V^*$ ,  $B : V \rightarrow Z^*$ , and  $C : Z \rightarrow Z^*$ . Assume that:

- i)  $A$  is elliptic, i.e., there exists  $\alpha > 0$  such that  $\langle A(v), v \rangle_V \geq \alpha \|v\|_V^2$  for all  $v \in V$ ,
- ii)  $B$  is surjective, i.e., there exists  $\beta > 0$  such that  $\|B^*(z)\|_V \geq \beta \|z\|_Z$  for all  $z \in Z$ ,
- iii)  $C$  is positive semidefinite, i.e.,  $\langle C(z), z \rangle \geq 0 \quad \forall z \in Z$ .

Then,  $\mathbb{T}$  is bijective.

*Proof.* See [19, Lemma 3.4] and [18, Lemma 2.1]. □

### 3.2 Well-posedness

Our analysis of the poroelasticity problem (4) is built upon a key assumption. Specifically, we suppose that the underlying elasticity equation is well-posed at the continuous level in the space  $\mathbf{H}$ . To formally introduce this hypothesis, we define the scalar products on  $\mathbf{H}$  as follows:

$$(\mathbf{v}, \mathbf{w})_{0,\rho} := \rho(\mathbf{v}, \mathbf{w})_\Omega$$

$$\begin{aligned} (\mathbf{v}, \mathbf{w})_{1, \mu_e} &:= 2\mu_e (\epsilon(\mathbf{v}), \epsilon(\mathbf{w}))_{\Omega} \\ (\mathbf{v}, \mathbf{w})_{1, \mu_e, \rho} &:= (\mathbf{v}, \mathbf{w})_{1, \mu_e} + (\mathbf{v}, \mathbf{w})_{0, \rho} \end{aligned}$$

Here  $\mathbf{v}, \mathbf{w} \in \mathbf{H}$ , and denote the associated norms as  $\|\mathbf{v}\|_{0, \rho}$ ,  $\|\mathbf{v}\|_{1, \mu_e}$ , and  $\|\mathbf{v}\|_{1, \mu_e, \rho}$ .

Given that  $\Omega$  is bounded and assuming that the boundary  $\partial\Omega$  is sufficiently regular, one can conclude that  $\mathbf{H}$  is compactly embedded into  $L^2(\Omega)^d$  (see, e.g., [15]). Therefore, there exists a Hilbert basis of  $L^2(\Omega)^d$  composed of eigenfunctions of the elasticity operator, i.e., there exists a family  $(\mathbf{v}_n, \lambda_n)_n \in \mathbf{H} \times \mathbb{R}^+$  such that  $\mathbf{v}_n \neq \mathbf{0}$  and

$$\begin{aligned} (\mathbf{v}_n, \mathbf{w})_{1, \mu_e} &= \lambda_n (\mathbf{v}_n, \mathbf{w})_{0, \rho} \quad \forall \mathbf{w} \in \mathbf{H}, \\ \lim_{n \rightarrow \infty} \lambda_n &= +\infty, \\ \|\mathbf{v}_n\|_{1, \mu_e, \rho} &= 1. \end{aligned} \tag{29}$$

Hence, for any  $\mathbf{v} \in \mathbf{H}$ , it holds

$$\mathbf{v} = \sum_{n \geq 0} \alpha_n \mathbf{v}_n, \quad \alpha_n := (\mathbf{v}, \mathbf{v}_n)_{1, \mu_e, \rho},$$

$$\text{and } \|\mathbf{v}\|_{1, \mu_e, \rho}^2 = \sum_{n \geq 0} \alpha_n^2.$$

Our assumption is then formulated as follows.

**Assumption 1** (Well-posedness of the underlying elasticity problem). *Let  $\lambda_n$  be the eigenvalues introduced in (29). We assume that*

$$(i) \quad \omega^2 \notin (\lambda_n)_{n \geq 0},$$

$$(ii) \quad \text{There exists } \bar{m} \in \mathbb{N} \mid \bar{m} = \max\{n \in \mathbb{N} \mid \omega^2 > \lambda_n\}.$$

Firstly, we show the continuity of  $\mathcal{A}$  and  $\mathcal{F}$  in the chosen norm.

**Lemma 7** (Continuity). *There exist two constants  $\eta_1, \eta_2 > 0$ , depending on the physical and geometrical problem parameters such that*

$$\|\mathcal{A}(\vec{\mathbf{u}})\|_{\mathcal{U}} \leq \eta_1 \|\vec{\mathbf{u}}\|_{\mathcal{U}} \tag{30}$$

and

$$\|\mathcal{F}\|_{\mathcal{U}} \leq \eta_2 \left( \|\mathbf{g}_{re}^u\|_{0, \Gamma_p} + \|\mathbf{g}_{re}^p\|_{0, \Gamma_u} \right) \tag{31}$$

*Proof.* The results follow from the Cauchy-Schwarz inequality and from the inequality (26). One ob-

tains:

$$\begin{aligned}
& |\langle \mathcal{A}(\vec{\mathbf{u}}), \vec{\mathbf{v}} \rangle| \leq \\
& \omega^2 \rho \|\mathbf{u}\|_0 \|\mathbf{v}\|_0 + 2\mu_e \|\varepsilon(\mathbf{u})\|_0 \|\varepsilon(\mathbf{v})\|_0 + \frac{\theta}{\lambda} \|p\|_0 \|q\|_0 + \frac{\kappa}{\mu_f \omega \alpha} \|\nabla p\|_0 \|\nabla q\|_0 \\
& + \|\phi\|_0 \|\nabla \cdot \mathbf{v}\|_0 + \|\phi\|_0 \|q\|_0 + \|\nabla \cdot \mathbf{u}\|_0 \|\xi\|_0 + \lambda^{-1} \|\phi\|_0 \|\xi\|_0 + \lambda^{-1} \|p\|_0 \|\xi\|_0 \\
& \leq \left( \frac{\omega^2 \rho (C_P C_K)^2}{2\mu_e} + 1 \right) 2\mu_e \|\varepsilon(\mathbf{u})\|_0 \|\varepsilon(\mathbf{v})\|_0 + \left( \frac{\theta}{\lambda} \left( \frac{\kappa}{\mu_f \omega \alpha} \right)^{-1} + C_P \right) \frac{\kappa}{\mu_f \omega \alpha} \|p\|_1 \|q\|_1 \\
& + \frac{\lambda^{1/2} C_K \sqrt{d}}{\sqrt{2\mu_e}} \lambda^{-1/2} \|\phi\|_0 \sqrt{2\mu_e} \|\varepsilon(\mathbf{v})\|_0 + \alpha \lambda^{1/2} \left( \frac{\kappa}{\mu_f \omega \alpha} \right)^{-1/2} \lambda^{-1/2} \|\phi\|_0 \left( \frac{\kappa}{\mu_f \omega \alpha} \right)^{1/2} \|q\|_1 \\
& + \frac{\lambda^{3/2} C_K \sqrt{d}}{\sqrt{2\mu_e}} \sqrt{2\mu_e} \|\varepsilon(\mathbf{u})\|_0 \lambda^{-1/2} \|\xi\|_0 + \lambda^{-1} \|\phi\|_0 \|\xi\|_0 \\
& + \alpha \lambda^{-1/2} \left( \frac{\kappa}{\mu_f \omega \alpha} \right)^{-1/2} \left( \frac{\kappa}{\mu_f \omega \alpha} \right)^{1/2} \|p\|_1 \lambda^{-1/2} \|\xi\|_0 \\
& \leq \eta_1 \|\vec{\mathbf{u}}\|_U \|\vec{\mathbf{v}}\|_U
\end{aligned} \tag{32}$$

where

$$\begin{aligned}
\eta_1 = 3 \max & \left\{ \frac{\omega^2 \rho (C_P C_K)^2}{2\mu_e} + 1, \frac{\theta}{\lambda} \left( \frac{\kappa}{\mu_f \omega \alpha} \right)^{-1} + C_P, \frac{\lambda^{1/2} C_K \sqrt{d}}{\sqrt{2\mu_e}}, \right. \\
& \left. \lambda^{1/2} \left( \frac{\kappa}{\mu_f \omega \alpha} \right)^{-1/2}, \frac{\lambda^{3/2} C_K \sqrt{d}}{\sqrt{2\mu_e}}, \lambda^{-1/2} \left( \frac{\kappa}{\mu_f \omega \alpha} \right)^{-1/2} \right\}.
\end{aligned}$$

For the right hand side, it holds

$$\begin{aligned}
\langle \mathcal{F}, \vec{\mathbf{v}} \rangle & \leq \|g^u\|_{0,\Gamma_p} \|\mathbf{v}\|_{0,\Gamma_p} + \|g^p\|_{0,\Gamma_u} \|q\|_{0,\Gamma_u} \\
& \leq C_{tr}^1 \|g^u\|_{0,\Gamma_p} \|\mathbf{v}\|_1 + \frac{C_{tr}^2}{\omega} \|g^p\|_{0,\Gamma_u} \|q\|_1,
\end{aligned}$$

where we have used the inequalities (25) and (26). The estimate (31) follows then from the Cauchy-Schwarz inequality, i.e.,

$$\langle \mathcal{F}, \vec{\mathbf{v}} \rangle \leq \eta_2 \left( \|g^u\|_{0,\Gamma_p}^2 + \|g^p\|_{0,\Gamma_u}^2 \right)^{1/2} \left( \|\mathbf{v}\|_1^2 + \|q\|_1^2 \right)^{1/2} \leq \eta_2 \left( \|g^u\|_{0,\Gamma_p} + \|g^p\|_{0,\Gamma_u} \right) \|\vec{\mathbf{v}}\|_U,$$

where

$$\eta_2 = C_{tr} \max \left\{ (2\mu_e)^{-1/2}, \left( \frac{\kappa}{\mu_f \omega \alpha} \right)^{-1/2} \frac{1}{\omega^2} \right\}. \tag{33}$$

□

Let  $(\mathbf{v}_n)$  be the eigenvectors introduced in (29). Let us now consider the index  $\bar{m}$  introduced in Assumption 1 and the subspace

$$\mathbf{H}^- := \text{span}_{0 \leq n \leq \bar{m}}(\mathbf{v}_n).$$

Let  $\Pi_{\mathbf{H}^-}$  be the orthogonal projection on  $\mathbf{H}^-$  and let  $\mathbb{T} := \mathbb{I}_{\mathbf{H}} - 2\Pi_{\mathbf{H}^-}$ , where  $\mathbb{I}_{\mathbf{H}}$  is the identity on  $\mathbf{H}$ .

**Lemma 8.** Let  $a_1(\cdot, \cdot)$  be the bilinear form introduced in (12). Under the hypotheses of Assumption 1 it holds

- (i)  $a_1(\cdot, \cdot)$  is  $\mathbb{T}$ -coercive, and  
(ii) the bilinear form  $(\mathbf{u}, \mathbf{v}) \mapsto a_1(\mathbf{u}, \Pi_{\mathbf{H}^-}(\mathbf{v}))$  is positive definite, i.e.,

$$a_1(\mathbf{v}, \Pi_{\mathbf{H}^-}(\mathbf{v})) > 0, \forall \mathbf{v} \in \mathbf{H}. \quad (34)$$

*Proof.* The proof follows the approach presented in [10]. First, it is noteworthy that, based on the definition of  $\mathbb{T}$ , one can derive

$$\mathbb{T}\mathbf{v}_n = \begin{cases} -\mathbf{v}_n, & 0 \leq n \leq \bar{m} \\ +\mathbf{v}_n, & n > \bar{m}. \end{cases}$$

Thus,  $\mathbb{T}^2 = \mathbb{I}$ , implying that  $\mathbb{T}$  is bijective. For the  $\mathbb{T}$ -coercivity, it shall be proven that there exists a constant  $\alpha_{min}$  depending on  $\omega$  and  $(\lambda_n)_{n \geq 0}$  such that

$$a_1(\mathbf{v}, \mathbb{T}(\mathbf{v})) \geq \alpha_{min} \|\mathbf{v}\|_{1, \mu_e, \rho}^2$$

for all  $\mathbf{v} \in \mathbf{H}$ .

To this end, we follow [10, Prop. 1], which allows to obtain

$$\begin{aligned} a_1(\mathbf{v}, \mathbb{T}(\mathbf{v})) &= \sum_{0 \leq n \leq \bar{m}} \alpha_n a_1(\mathbf{v}, (\mathbb{T}(\mathbf{v}_n))) + \sum_{n > \bar{m}} \alpha_n a_1(\mathbf{v}, (\mathbb{T}(\mathbf{v}_n))) \\ &= \sum_{0 \leq n \leq \bar{m}} \alpha_n a_1(\mathbf{v}, -\mathbf{v}_n) + \sum_{n > \bar{m}} \alpha_n a_1(\mathbf{v}, \mathbf{v}_n) \\ &= \sum_{0 \leq n \leq \bar{m}} \alpha_n [\omega^2(\mathbf{v}, \mathbf{v}_n)_{0, \rho} - (\mathbf{v}, \mathbf{v}_n)_{1, \mu_e}] + \sum_{n > \bar{m}} \alpha_n [(\mathbf{v}, \mathbf{v}_n)_{1, \mu_e} - \omega^2(\mathbf{v}, \mathbf{v}_n)_{0, \rho}] \\ &= \sum_{0 \leq n \leq \bar{m}} \left( \frac{\omega^2 - \lambda_n}{1 + \lambda_n} \right) \alpha_n^2 + \sum_{n > \bar{m}} \left( \frac{\lambda_n - \omega^2}{1 + \lambda_n} \right) \alpha_n^2 \geq \alpha_{min} \|\mathbf{v}\|_{1, \mu_e, \rho}^2 \end{aligned} \quad (35)$$

with  $\alpha_{min} = \min_{n \geq 0} \left| \frac{\omega^2 - \lambda_n}{1 + \lambda_n} \right|$ .

The inequality (34) can be demonstrated using analogous steps. One obtains

$$\begin{aligned} a_1(\mathbf{v}, \Pi_{\mathbf{H}^-}(\mathbf{v})) &= \sum_{0 \leq n \leq m} \alpha_n a_1(\mathbf{v}, (\Pi_{\mathbf{H}^-}(\mathbf{v}_n))) = \sum_{0 \leq n \leq m} \alpha_n a_1(\mathbf{v}, \mathbf{v}_n) = \\ &= \sum_{0 \leq n \leq m} \alpha_n [\omega^2(\mathbf{v}, \mathbf{v}_n)_{0, \rho} - (\mathbf{v}, \mathbf{v}_n)_{1, \mu_e}] \\ &= \sum_{0 \leq n \leq m} \left( \frac{\omega^2 - \lambda_n}{1 + \lambda_n} \right) \alpha_n^2 \geq \tilde{\alpha}_{min} \sum_{0 \leq n \leq m} \alpha_n^2 > 0, \end{aligned} \quad (36)$$

where  $\tilde{\alpha}_{min} = \min_{n \geq 0} \frac{\omega^2 - \lambda_n}{1 + \lambda_n}$ , and  $\tilde{\alpha}_{min} \neq 0$  due to Assumption 1 and the properties (29). □

**Lemma 9.** Let  $a_1(\cdot, \cdot)$  and  $a_2(\cdot, \cdot)$  be the bilinear forms introduced in equations (12) and (13), respectively. The bilinear form  $a(\cdot, \cdot) : (\mathbf{H} \times P) \times (\mathbf{H} \times P) \rightarrow \mathbb{C}$ , defined by

$$a((\mathbf{u}, p); (\mathbf{v}, q)) := a_1(\mathbf{u}, \mathbf{v}) + a_2(p, q),$$

for  $(\mathbf{u}, p), (\mathbf{v}, q) \in \mathbf{H} \times P$ , is elliptic.

*Proof.* Let  $(\mathbf{v}, q) \in \mathbf{H} \times P$ . From  $\mathbb{T} + 2\Pi_{\mathbf{H}^-} = \mathbb{I}_{\mathbf{H}}$  it follows that

$$\operatorname{Re} a_1(\mathbf{v}, \mathbf{v}) = \operatorname{Re} a_1(\mathbf{v}, \mathbb{T}(\mathbf{v})) + 2 \operatorname{Re} a_1(\mathbf{v}, \Pi_{\mathbf{H}^-}(\mathbf{v})), \quad (37)$$

for all  $\mathbf{v} \in \mathbf{H}$ . Using Lemma 8 and inequality (25) one obtains

$$\operatorname{Re} a_1(\mathbf{v}, \mathbf{v}) + \operatorname{Re} a_2(q, q) = \alpha_{\min} 2\mu_e \|\varepsilon(\mathbf{v})\|_0^2 + \frac{\kappa}{\omega \alpha \mu_f} \|\nabla q\|_0^2 \geq \tilde{\alpha} \left( 2\mu_e \|\varepsilon(\mathbf{v})\|_0^2 + \frac{\kappa}{\mu_f \omega \alpha} \|q\|_1^2 \right), \quad (38)$$

with

$$\tilde{\alpha} = \min \{ \alpha_{\min}, C_P^{-1} \}. \quad (39)$$

□

**Lemma 10.** *The bilinear form  $\tilde{b}$  defined in (14) satisfies a continuous inf-sup condition, i.e., there exists  $\beta_1 > 0$  such that*

$$\sup_{\substack{\mathbf{v} \in \mathbf{H} \\ \mathbf{v} \neq \mathbf{0}}} \frac{\tilde{b}(\mathbf{v}, \xi)}{\|\mathbf{v}\|_1} \geq \beta_1 \|\xi\|_0, \quad (40)$$

for all  $\xi \in S$ .

*Proof.* See, e.g., [20].

□

The previous results allow to prove the first main result.

**Lemma 11.** *The operator  $\mathcal{B}$  defined in equation (22) is bijective.*

*Proof.* The proof relies on decomposing the operator  $\mathcal{B}$  as in (28). We observe that, for all  $\xi \in S$  it holds

$$\operatorname{Re} d(\xi, \xi) = \lambda^{-1} \|\xi\|_0^2 \geq 0.$$

Combining this result with Lemma 9 and Lemma 10 allows us to infer bijectivity of  $\mathcal{B}$  using Theorem 6. □

**Lemma 12.** *The operator  $\mathcal{C}$ , defined in equation (23), is compact.*

*Proof.* The compactness of  $\mathcal{C}$  follows from the fact that  $\mathbb{C} = \lambda^{-1} I \circ i_c$ , where  $I : L^2(\Omega) \rightarrow L^2(\Omega)$  and  $i_c$  represents the identity operator along with the compact embedding from  $H^1(\Omega)$  into  $L^2(\Omega)$  (for details, see [28, Lemma 2.2]). □

**Lemma 13.** *Under the hypothesis of Assumption (1), the operator  $\mathcal{A}$  is injective.*

*Proof.* Let  $\vec{\mathbf{v}} \in \mathbf{U}$  such that  $\mathcal{A}(\vec{\mathbf{v}}) = 0$ , i.e.,

$$\operatorname{Re} \langle \mathcal{A}(\vec{\mathbf{v}}), \vec{\mathbf{v}} \rangle = \operatorname{Im} \langle \mathcal{A}(\vec{\mathbf{v}}), \vec{\mathbf{v}} \rangle = 0.$$

From

$$\begin{aligned} \langle \mathcal{A}(\vec{\mathbf{v}}), \vec{\mathbf{v}} \rangle &= -\omega^2 \rho \|\mathbf{v}\|_0^2 + 2\mu_e \|\varepsilon(\mathbf{v})\|_0^2 + i\theta \lambda^{-1} \|q\|_0^2 + \frac{\kappa}{\mu_f \omega \alpha} \|\nabla q\|_0^2 \\ &\quad - i\lambda^{-1} (\xi, q) - \lambda^{-1} (q, \xi) + \lambda^{-1} \|\xi\|_0^2. \end{aligned}$$

one obtains ( $\lambda \in \mathbb{R}$ )

$$\operatorname{Im}\langle \mathcal{A}(\vec{v}), \vec{v} \rangle = 0 \Leftrightarrow \theta \lambda^{-1} \|q\|_0^2 - \lambda^{-1} \operatorname{Re}(\xi, q) - \lambda^{-1} \operatorname{Im}(q, \xi) = 0,$$

and hence, using  $(q, \xi) = (\xi, q)$ ,

$$\lambda^{-1} \operatorname{Im}(\xi, q) = \lambda^{-1} \theta \|q\|_0^2 - \lambda^{-1} \operatorname{Re}(\xi, q) \quad (41)$$

Analogously, from  $\operatorname{Re}\langle \mathcal{A}(\vec{v}), \vec{v} \rangle = 0$ , one obtains

$$\begin{aligned} 0 &= -\omega^2 \rho \|\mathbf{v}\|_0^2 + 2\mu_e \|\varepsilon(\mathbf{v})\|_0^2 + \frac{\kappa}{\mu_f \omega \alpha} \|\nabla q\|_0^2 + \lambda^{-1} \operatorname{Im}(\xi, q) - \lambda^{-1} \operatorname{Re}(\xi, q) + \lambda^{-1} \|\xi\|_0^2 \\ &\stackrel{(41)}{=} -\omega^2 \rho \|\mathbf{v}\|_0^2 + 2\mu_e \|\varepsilon(\mathbf{v})\|_0^2 + \frac{\kappa}{\mu_f \omega \alpha} \|\nabla q\|_0^2 + \lambda^{-1} \theta \|q\|_0^2 - 2\lambda^{-1} \operatorname{Re}(\xi, q) + \lambda^{-1} \|\xi\|_0^2 \\ &\stackrel{(5)}{=} -\omega^2 \rho \|\mathbf{v}\|_0^2 + 2\mu_e \|\varepsilon(\mathbf{v})\|_0^2 + \frac{\kappa}{\mu_f \omega \alpha} \|\nabla q\|_0^2 + \frac{S_\epsilon}{\alpha} \|q\|_0^2 + \lambda^{-1} \|q\|_0^2 \\ &\quad - 2\lambda^{-1} \operatorname{Re}(\xi, q) + \lambda^{-1} \|\xi\|_0^2 \\ &= -\omega^2 \rho \|\mathbf{v}\|_0^2 + 2\mu_e \|\varepsilon(\mathbf{v})\|_0^2 + \frac{\kappa}{\mu_f \omega \alpha} \|\nabla q\|_0^2 + \frac{S_\epsilon}{\alpha} \|q\|_0^2 + \lambda^{-1} (\|q\|_0^2 - 2 \operatorname{Re}(\xi, q) + \|\xi\|_0^2). \end{aligned} \quad (42)$$

Hence, from

$$\operatorname{Re}(\xi, q) \leq \|\xi\|_0 \|q\|_0 \leq \frac{1}{2} \|\xi\|_0^2 + \frac{1}{2} \|q\|_0^2 \quad (43)$$

and Lemma 9 one obtains

$$0 \geq 2\mu_e \alpha_{\min} \|\varepsilon(\mathbf{v})\|_0^2 + \frac{\kappa}{\mu_f \omega \alpha} \|\nabla q\|_0^2 + \frac{S_\epsilon}{\alpha} \|q\|_0^2 \quad (44)$$

which is satisfied only for  $(\mathbf{v}, q) = (\mathbf{0}, 0)$ . At the same time,  $(\mathbf{v}, q) = (\mathbf{0}, 0)$  yields

$$0 = \langle \mathcal{A}(\vec{v}), \vec{v} \rangle = \lambda^{-1} \|\xi\|_0^2$$

and thus  $\xi = 0$ , concluding the proof.  $\square$

Using Lemmas 11, 12, 13 and the Fredholm's alternative allows to state the main stability result.

**Theorem 14** (Well-posedness). *The problem (19) has a unique solution  $\vec{u}^* \in \mathcal{U}$ , and there exists a positive constant  $C$  such that there holds*

$$\|\vec{u}^*\|_{\mathcal{U}} \leq C \|\mathcal{F}\|_{\mathcal{U}} \leq C \left[ \|g^p\|_{0, \Gamma_u} + \|g_{re}\|_{0, \Gamma_p} \right]. \quad (45)$$

**Remark 1.** Note that (45) is equivalent to the following inf-sup condition:

$$\exists \beta_2 > 0 : \inf_{\substack{\vec{u} \in \mathcal{U} \\ \vec{u} \neq \vec{0}}} \sup_{\substack{\vec{v} \in \mathcal{U} \\ \vec{v} \neq \vec{0}}} \frac{|\langle \mathcal{A}(\vec{u}), \vec{v} \rangle|}{\|\vec{v}\|_{\mathcal{U}} \|\vec{u}\|_{\mathcal{U}}} \geq \beta_2. \quad (46)$$

## 4 Analysis of the discrete problem

This section is dedicated to the well-posedness and stability analysis of the discrete problem arising using a stabilized finite element formulation of (19).

## 4.1 Stabilized finite element formulation

Let  $\{\mathcal{T}_h\}_{h>0}$  denote a shape-regular triangulation of  $\bar{\Omega}$ . For an element  $T \in \mathcal{T}_h$  we denote with  $h_T$  the diameter, introducing

$$h := \max\{h_T : T \in \mathcal{T}_h\}$$

as the characteristic mesh size. Let us also assume that there exist a constant  $h_0 > 0$  such that  $h \leq h_0$ , for all triangulations. Denoting  $\mathcal{P}_j(T)$  ( $j \in \mathbb{N}$ ) as the space of polynomials of total degree less than or equal to  $j$  over an element  $T \in \mathcal{T}_h$ , we define the following continuous finite element spaces:

$$\begin{aligned} \mathbf{H}_h &:= \{\mathbf{v}^h \in C(\bar{\Omega})^d : \mathbf{v}^h|_T \in \mathcal{P}_k(T)^d, \forall T \in \mathcal{T}_h\} \cap \mathbf{H} \\ P_h &:= \{q^h \in C(\bar{\Omega}) : q^h|_T \in \mathcal{P}_l(T), \forall T \in \mathcal{T}_h\} \cap P \\ S_h &:= \{\xi^h \in C(\bar{\Omega}) : \xi^h|_T \in \mathcal{P}_m(T), \forall T \in \mathcal{T}_h\} \end{aligned} \quad (47)$$

and let  $\mathbf{U}_h \equiv \mathbf{H}_h \times P_h \times S_h$ . The analysis presented in the following part can be applied to general finite element triples. However, we focus on the case of equal-order elements, i.e., choosing  $k = l = m$ .

It is well known that, in this case, the discrete spaces do not satisfy an inf-sup condition. For this reason, the discrete formulation will be equipped with additional stabilizations. On the other hand, the choice of equal order elements is motivated by the reduced computational cost, particularly evident in realistic three-dimensional examples.

For the stabilized methods, we consider the residual of the momentum equation:

$$\mathbf{R}(\mathbf{v}^h, \xi^h) := \omega^2 \rho \mathbf{v}^h + 2\mu_e \operatorname{div} \varepsilon(\mathbf{v}^h) - \nabla \xi^h. \quad (48)$$

Additionally, we introduce an additional term inspired by the Brezzi-Pitkäranta stabilization (see [8]) and define the operator  $\mathcal{S}_h : \mathbf{U}_h \rightarrow \mathbf{U}_h^*$  as follows:

$$\langle \mathcal{S}_h(\vec{\mathbf{u}}^h), \vec{\mathbf{v}}^h \rangle := \delta_1 \sum_{T \in \mathcal{T}_h} h_T^2 (\mathbf{R}(\mathbf{u}^h, \phi^h), \mathbf{R}(\mathbf{v}^h, \xi^h))_T + \delta_2 \sum_{T \in \mathcal{T}_h} \frac{h_T^2}{\mu_f \alpha \omega} (\nabla p^h, \nabla q^h)_T, \quad (49)$$

where  $\delta_1 > 0$  and  $\delta_2 \geq 0$  are two stabilization parameters.

Both terms are designed to address the lack of inf-sup stability in the finite element spaces. In particular, the second term can be seen as an artificial permeability which becomes relevant only for small values of  $\kappa$  and it aims to handle instabilities that may arise in the low permeability range (see, e.g., [31], [40]).

**Remark 2.** For clarity, the Brezzi-Pitkäranta term is only necessary for small values of  $\kappa$ , i.e., when  $\kappa \ll 1$ . Otherwise, it suffices to consider  $\delta_2 = 0$ .

The proposed finite element formulation reads:

**Problem 1.** Find  $\vec{\mathbf{u}}^h = (\mathbf{u}^h, p^h, \phi^h) \in \mathbf{U}_h$  such that

$$\langle \mathcal{A}_h(\vec{\mathbf{u}}^h), \vec{\mathbf{v}}^h \rangle = \langle \mathcal{F}, \vec{\mathbf{v}}^h \rangle, \quad \forall \vec{\mathbf{v}}^h \in \mathbf{U}_h, \quad (50)$$

where

$$\mathcal{A}_h := \mathcal{B} + \mathcal{S}_h + \mathcal{C}. \quad (51)$$

## 4.2 Well-posedness of the discrete problem

The well-posedness of problem (50) will be addressed based on the decomposition (51), following an argument analogous to the one used in Section 3.

First, let us define the following mesh-dependent norm over  $U_h$ :

$$\|\vec{v}^h\|_{U_h}^2 := \|\vec{v}^h\|_U^2 + \delta_1 \sum_{T \in \mathcal{T}_h} h_T^2 \|\mathbf{R}(\mathbf{v}^h, \xi^h)\|_{0,T}^2 + \delta_2 \sum_{T \in \mathcal{T}_h} \frac{h_T^2}{\mu_f \alpha \omega} \|\nabla q\|_{0,T}^2. \quad (52)$$

In what follows, we will also use the following inverse inequalities: there exist two constants  $C_I$  and  $\tilde{C}_I$  such that

$$h_T^2 \|\operatorname{div} \varepsilon(\mathbf{v}^h)\|_{0,T}^2 \leq C_I^2 \|\varepsilon(\mathbf{v}^h)\|_{0,T}^2, \quad (53)$$

and

$$h_T^2 \|\nabla \mathbf{v}^h\|_{0,T}^2 \leq \tilde{C}_I^2 \|\mathbf{v}^h\|_{0,T}^2, \quad (54)$$

for any element  $T$  in the triangulation and for all  $\mathbf{v}^h \in \mathbf{H}_h$ .

We begin stating a result analogous to Theorem 5, valid for the discrete setting.

**Theorem 15.** *Let  $(V_h)_h$  and  $(W_h)_h$  be two families of finite dimensional Hilbert spaces such that  $\dim V_h = \dim W_h$ ,  $\forall h$ , and let  $(L_h)_h$  a family of operators  $L_h : V_h \rightarrow W_h$ , uniformly bounded in  $h$ . Then, the followings statements are equivalent:*

- (i) *The problem  $L_h u_h = f$  is well-posed and  $(L_h^{-1})_h$  is uniformly bounded;*
- (ii)  *$(L_h)_h$  is  $T$ -coercive.*

*Proof.* See [10, Th. 2]. □

The following lemma concerns the orthogonality of the Galerkin finite element method, which is only achieved asymptotically ( $\sim O(h^2)$ ) or when  $\delta_2 = 0$ .

**Lemma 16** ( $h^2$ -Galerkin Orthogonality). *Let  $\vec{u}$  and  $\vec{u}^h$  be the solutions of (19) and (50), respectively. Assume that  $\mathbf{u} \in \mathbf{H} \cap H^2(\Omega)^d$ ,  $p \in p \cap H^2(\Omega)$ , and  $\phi \in S \cap H^1(\Omega)$ . Then, it holds*

$$\langle \mathcal{A}_h(\vec{u} - \vec{u}^h), \vec{v}^h \rangle = \delta_2 \sum_{T \in \mathcal{T}_h} \frac{h_T^2}{\mu_f \alpha \omega} (\nabla p, \nabla q^h)_T, \quad (55)$$

for all  $\vec{v}^h \in U_h$ .

*Proof.* It holds

$$\langle \mathcal{A}_h(\vec{u} - \vec{u}^h), \vec{v}^h \rangle = \langle \mathcal{A}(\vec{u}), \vec{v}^h \rangle + \langle \mathcal{S}_h(\vec{u}), \vec{v}^h \rangle - \langle \mathcal{A}_h(\vec{u}^h), \vec{v}^h \rangle = \mathcal{S}_h(\vec{u}).$$

Using the assumption on the regularity of the solution of (19), i.e.,  $\mathbf{u} \in \mathbf{H} \cap H^2(\Omega)^d$  and  $\phi \in S \cap H^1(\Omega)$ , one can conclude that  $\omega^2 \rho \mathbf{u} + 2\mu_e \operatorname{div} \varepsilon(\mathbf{u}) - \nabla \phi = 0$ , and hence

$$\mathcal{S}_h(\vec{u}) = \delta_2 \sum_{T \in \mathcal{T}_h} \frac{h_T^2}{\mu_f \alpha \omega} (\nabla p, \nabla q^h)_T.$$

□

The next lemma shows the continuity of the stabilized finite element operator  $\mathcal{A}_h$ .

**Lemma 17** (Continuity of  $\mathcal{A}_h$ ). *There exist two positive constants  $\eta_3$  and  $\eta_4$  such that, for any  $\vec{\mathbf{u}}^h \in \mathbf{U}_h$ , we have*

$$\|\mathcal{S}_h(\vec{\mathbf{u}}^h)\| \leq \eta_3 \|\vec{\mathbf{u}}^h\|_{\mathbf{U}} \quad \text{and} \quad \|\mathcal{A}_h(\vec{\mathbf{u}}^h)\| \leq \eta_4 \|\vec{\mathbf{u}}^h\|_{\mathbf{U}}.$$

*Proof.* Let  $\vec{\mathbf{u}}^h, \vec{\mathbf{v}}^h \in \mathbf{U}_h$ . Using the inverse inequalities (53) ad (54) we obtain

$$\begin{aligned} & \delta_1 \sum_{T \in \mathcal{T}_h} h_T^2 (\omega^2 \rho \mathbf{u}^h + 2\mu_e \operatorname{div} \varepsilon(\mathbf{u}^h) - \nabla \phi^h, \omega^2 \rho \mathbf{v}^h + 2\mu_e \operatorname{div} \varepsilon(\mathbf{v}^h) - \nabla \xi^h)_T \\ & \leq \delta_1 \sum_{T \in \mathcal{T}_h} h_T^2 \left( \omega^2 \rho \|\mathbf{u}^h\|_{0,T} + 2\mu_e \|\operatorname{div} \varepsilon(\mathbf{u}^h)\|_{0,T} + \|\nabla \phi^h\|_{0,T} \right) \times \\ & \quad \left( \omega^2 \rho \|\mathbf{v}^h\|_{0,T} + 2\mu_e \|\operatorname{div} \varepsilon(\mathbf{v}^h)\|_{0,T} + \|\nabla \xi^h\|_{0,T} \right) \\ & \leq \delta_1 \sum_{T \in \mathcal{T}_h} \left( \omega^2 \rho h_T \|\mathbf{u}^h\|_{0,T} + 2\mu_e C_I \|\varepsilon(\mathbf{u}^h)\|_{0,T} + \tilde{C}_I \|\phi^h\|_{0,T} \right) \times \\ & \quad \left( \omega^2 \rho h_T \|\mathbf{v}^h\|_{0,T} + 2\mu_e C_I \|\varepsilon(\mathbf{v}^h)\|_{0,T} + \tilde{C}_I \|\xi^h\|_{0,T} \right) \\ & \leq \delta_1 \max \left\{ \omega^2 \rho h_0 (2\mu)^{-1/2}, (2\mu_e)^{1/2} C_I, \tilde{C}_I \lambda^{1/2} \right\}^2 \\ & \quad \left[ \sum_{T \in \mathcal{T}_h} \left( (2\mu_e)^{1/2} \|\mathbf{u}^h\|_{0,T} + (2\mu_e)^{1/2} \|\varepsilon(\mathbf{u}^h)\|_{0,T} + \lambda^{-1/2} \|\phi^h\|_{0,T} \right)^2 \right]^{1/2} \times \\ & \quad \left[ \sum_{T \in \mathcal{T}_h} \left( (2\mu_e)^{1/2} \|\mathbf{v}^h\|_{0,T} + (2\mu_e)^{1/2} \|\varepsilon(\mathbf{v}^h)\|_{0,T} + \lambda^{-1/2} \|\xi^h\|_{0,T} \right)^2 \right]^{1/2} \\ & \leq 3\delta_1 \max \left\{ \omega^2 \rho h_0 (2\mu)^{-1/2}, (2\mu_e)^{1/2} C_I, \tilde{C}_I \lambda^{1/2} \right\}^2 \\ & \quad \left[ \sum_{T \in \mathcal{T}_h} \left( 2\mu_e \|\mathbf{u}^h\|_{0,T}^2 + 2\mu_e \|\varepsilon(\mathbf{u}^h)\|_{0,T}^2 + \lambda^{-1} \|\phi^h\|_{0,T}^2 \right) \right]^{1/2} \times \\ & \quad \left[ \sum_{T \in \mathcal{T}_h} \left( 2\mu_e \|\mathbf{v}^h\|_{0,T}^2 + 2\mu_e \|\varepsilon(\mathbf{v}^h)\|_{0,T}^2 + \lambda^{-1} \|\xi^h\|_{0,T}^2 \right) \right]^{1/2} \\ & = 3\delta_1 \max \left\{ \omega^2 \rho h_0 (2\mu)^{-1/2}, (2\mu_e)^{1/2} C_I, \tilde{C}_I \lambda^{1/2} \right\}^2 \left( 2\mu_e \|\mathbf{u}^h\|_0^2 + 2\mu_e \|\varepsilon(\mathbf{u}^h)\|_0^2 + \lambda^{-1} \|\phi^h\|_0^2 \right)^{1/2} \times \\ & \quad \left( 2\mu_e \|\mathbf{v}^h\|_0^2 + 2\mu_e \|\varepsilon(\mathbf{v}^h)\|_0^2 + \lambda^{-1} \|\xi^h\|_0^2 \right)^{1/2} \\ & \leq 3\delta_1 \max \left\{ \omega^2 \rho h_0 (2\mu)^{-1/2}, (2\mu_e)^{1/2} C_I, \tilde{C}_I \lambda^{1/2} \right\}^2 \\ & \quad \left( 2\mu_e (C_P C_K)^2 \|\varepsilon(\mathbf{u}^h)\|_0^2 + 2\mu_e \|\varepsilon(\mathbf{u}^h)\|_0^2 + \lambda^{-1} \|\phi^h\|_0^2 \right)^{1/2} \\ & \quad \left( 2\mu_e (C_P C_K)^2 \|\varepsilon(\mathbf{v}^h)\|_0^2 + 2\mu_e \|\varepsilon(\mathbf{v}^h)\|_0^2 + \lambda^{-1} \|\xi^h\|_0^2 \right)^{1/2} \\ & \leq 3\delta_1 \max \left\{ \omega^2 \rho h_0 (2\mu)^{-1/2}, (2\mu_e)^{1/2} C_I, \tilde{C}_I \lambda^{1/2}, \right\}^2 (1 + (C_P C_K)^2) \|\vec{\mathbf{u}}^h\|_{\mathbf{U}} \|\vec{\mathbf{v}}^h\|_{\mathbf{U}}. \end{aligned}$$

On the other hand,

$$\begin{aligned}
\delta_2 \sum_{T \in \mathcal{T}_h} \frac{h_T^2}{\mu_f \alpha \omega} (\nabla p^h, \nabla q^h)_T &\leq \delta_2 \sum_{T \in \mathcal{T}_h} \frac{h_T^2}{\mu_f \alpha \omega} \|\nabla p^h\|_{0,T} \|\nabla q^h\|_{0,T} \\
&\leq \delta_2 \left( \frac{h_0^2}{\kappa} \right) \frac{\kappa}{\mu_f \alpha \omega} \left( \sum_{T \in \mathcal{T}_h} \|\nabla p^h\|_{0,T}^2 \right)^{1/2} \left( \sum_{T \in \mathcal{T}_h} \|\nabla q^h\|_{0,T}^2 \right)^{1/2} \\
&\leq \delta_2 \left( \frac{h_0^2}{\kappa} \right) \|\vec{\mathbf{u}}^h\|_{\mathcal{U}} \|\vec{\mathbf{v}}^h\|_{\mathcal{U}}.
\end{aligned} \tag{56}$$

So, taking  $\eta_3 = 3\delta_1 \max \left\{ \omega^2 \rho h_0 (2\mu)^{-1/2}, (2\mu_e)^{1/2} C_I, \tilde{C}_I \lambda^{1/2} \right\}^2 (1 + (C_P C_K)^2) + \delta_2 \left( \frac{h_0^2}{\kappa} \right)$ , we arrive to

$$\|\mathcal{S}_h(\vec{\mathbf{u}}^h)\| \leq \eta_3 \|\vec{\mathbf{u}}^h\|_{\mathcal{U}} \tag{57}$$

Inequality (57) proves the continuity of  $\mathcal{S}_h$ . Combined with the continuity of  $\mathcal{A}$  shown in Lemma (7), we can conclude that  $\mathcal{A}_h$  is also continuous, i.e.,

$$\langle \mathcal{A}_h(\vec{\mathbf{u}}^h), \vec{\mathbf{v}}^h \rangle \leq \eta_4 \|\vec{\mathbf{u}}^h\|_{\mathcal{U}} \|\vec{\mathbf{v}}^h\|_{\mathcal{U}}, \tag{58}$$

with  $\eta_4 = \eta_1 + \eta_3$ .

□

From continuity, it follows that the discrete norm (52) is equivalent to the continuous norm (11). In fact, the inequality  $\|\vec{\mathbf{v}}\|_{\mathcal{U}_h}^2 \geq \|\vec{\mathbf{v}}\|_{\mathcal{U}}^2$  is straightforward. On the other hand, by taking  $h \leq h_0$  and appealing to the inequalities (56) and (56), we obtain

$$\|\vec{\mathbf{v}}^h\|_{\mathcal{U}_h}^2 = \|\vec{\mathbf{v}}^h\|_{\mathcal{U}}^2 + \delta_1 \sum_{T \in \mathcal{T}_h} h_T^2 \|\mathbf{R}(\mathbf{v}^h, \phi^h)\|_{0,T}^2 + \delta_2 \sum_{T \in \mathcal{T}_h} \frac{h_T^2}{\mu_f \alpha \omega} \|\nabla q\|_{0,T}^2 \leq (1 + \eta_3) \|\vec{\mathbf{v}}^h\|_{\mathcal{U}}^2. \tag{59}$$

As in the continuous case, the stability of the finite element method relies on the decomposition of the operator  $\mathcal{A}_h$  into an elliptic  $\mathcal{B} + \mathcal{S}_h$  and a compact operator  $\mathcal{C}$ . The compactness of  $\mathcal{C}$  in the discrete case follows with an argument analogous to Lemma 12. The next lemma shows the coercivity of the operator  $\mathcal{B} + \mathcal{S}_h$ .

**Lemma 18** (Coercivity of  $\mathcal{B} + \mathcal{S}_h$ ). *Let  $\mathcal{B}_h := \mathcal{B} + \mathcal{S}_h$ . There exists a positive constant  $\alpha_2$ , which depends on the frequency  $\omega$  and on the domain  $\Omega$ , such that*

$$\operatorname{Re} \langle \mathcal{B}_h(\vec{\mathbf{v}}^h), \vec{\mathbf{v}}^h \rangle \geq \alpha_2 \|\vec{\mathbf{v}}^h\|_{\mathcal{U}_h}^2. \tag{60}$$

*Proof.* Due to the fact that  $\mathbf{H}^-$  is of finite dimension, it is possible to construct a space  $\mathbf{H}_h^-$  such that the latter is an approximation of the former. This can be achieved by considering approximations  $(\mathbf{v}_n^h)_{0 \leq n \leq m}$  of the basis  $(\mathbf{v}_n)_{0 \leq n \leq m}$ . Therefore, we can define the space

$$\mathbf{H}_h^- = \operatorname{Span}_{0 \leq n \leq m}(\mathbf{v}_n^h).$$

Now, similar to the continuous case, we define  $\mathbb{T}_h := \mathbb{I}_{\mathbf{H}_h} - 2\mathbb{P}_h^-$  of  $\mathcal{L}(\mathbf{H}_h)$ , whose properties are studied in [10]. Although the analysis is omitted here, we can assert that under the construction of this discrete operator, the same result as in the continuous problem is achieved, as stated in Theorem (8).

By applying Theorem (15) for the discrete  $\mathbb{T}_h$ -coercivity of  $\mathbb{A}_1$ , we obtain

$$\begin{aligned} \operatorname{Re}\langle \mathcal{B}_h(\vec{\mathbf{v}}^h), \vec{\mathbf{v}}^h \rangle &= \operatorname{Re}\langle \mathbb{A}_1(\mathbf{v}^h), \mathbf{v}^h \rangle + \operatorname{Re}\langle \mathbb{A}_2(q^h), q^h \rangle + \operatorname{Re}\langle \tilde{\mathbb{D}}(\xi^h), \xi^h \rangle + \operatorname{Re}\langle \mathcal{S}(\vec{\mathbf{v}}^h), \vec{\mathbf{v}}^h \rangle \\ &\geq \alpha_1 \left( 2\mu_e \|\varepsilon(\vec{\mathbf{v}}^h)\|_0^2 + \frac{\kappa}{\mu_f \omega \alpha} \|q^h\|_1^2 \right) + \lambda^{-1} \|\xi^h\|_0^2 + \delta_1 \sum_{T \in \mathcal{T}_h} h_T^2 \|\mathbf{R}(\mathbf{v}^h, \xi^h)\|_{0,T}^2 \\ &\quad + \delta_2 \sum_{T \in \mathcal{T}_h} \frac{h_T^2}{\mu_f \alpha \omega} \|\nabla q^h\|_{0,T}^2 \\ &\geq \alpha_2 \|\vec{\mathbf{v}}^h\|_{\mathcal{U}_h}^2, \end{aligned}$$

where  $\alpha_2 = \min\{\alpha_1, 1\}$ .

□

Finally, the injectivity of  $\mathcal{A}_h$  is proven in the following lemma.

**Lemma 19** (Injectivity of  $\mathcal{A}_h$ ). *The operator  $\mathcal{A}_h$  is injective.*

*Proof.* Let  $\vec{\mathbf{v}}^h \in \mathcal{U}_h$  such that  $\mathcal{A}_h(\vec{\mathbf{v}}^h) = 0$ . Then,

$$\begin{aligned} 0 &= 2|\langle \mathcal{A}_h(\vec{\mathbf{v}}^h), \vec{\mathbf{v}}^h \rangle| \\ &\geq \operatorname{Re}\langle \mathcal{A}_h(\vec{\mathbf{v}}^h), \vec{\mathbf{v}}^h \rangle + \operatorname{Im}\langle \mathcal{A}_h(\vec{\mathbf{v}}^h), \vec{\mathbf{v}}^h \rangle \\ &= \langle \mathbb{A}_1(\vec{\mathbf{v}}^h), \vec{\mathbf{v}}^h \rangle + \operatorname{Re}\langle \mathbb{A}_2(q^h), q^h \rangle + \operatorname{Re}\langle \tilde{\mathbb{D}}(\xi^h), \xi^h \rangle + \lambda^{-1} \left( \operatorname{Im}(\xi, q) - \operatorname{Re}(\xi, q) \right) \\ &\quad + \theta \lambda^{-1} \|q^h\|_0^2 - \lambda^{-1} \left( \operatorname{Im}(\xi, q) + \operatorname{Re}(\xi, q) \right) + \operatorname{Re}\langle \mathcal{S}(\vec{\mathbf{v}}^h), \vec{\mathbf{v}}^h \rangle \\ &\geq \alpha_{\min} 2\mu_e \|\varepsilon(\vec{\mathbf{v}}^h)\|_0^2 + \frac{\kappa}{\alpha \omega \mu_f} \|\nabla q^h\|_0^2 + \lambda^{-1} \|\xi^h\|_0^2 - \lambda^{-1} \|\xi^h\|_0^2 - \lambda^{-1} \|q^h\|_0^2 + \frac{S_\varepsilon}{\alpha} \|q^h\|_0^2 \\ &\quad + \lambda^{-1} \|q^h\|_0^2 + \delta_1 \sum_{T \in \mathcal{T}_h} h_T^2 \|\mathbb{R}(\vec{\mathbf{v}}^h, \xi^h)\|_{0,T}^2 + \delta_2 \sum_{T \in \mathcal{T}_h} \frac{h_T^2}{\mu_f \alpha \omega} \|\nabla q^h\|_{0,T}^2 \\ &\geq \alpha_{\min} 2\mu_e \|\varepsilon(\vec{\mathbf{v}}^h)\|_0^2 + \frac{\kappa}{\alpha \omega \mu_f} \|\nabla q^h\|_0^2 + \delta_1 \sum_{T \in \mathcal{T}_h} h_T^2 \|\mathbb{R}(\vec{\mathbf{v}}^h, \xi^h)\|_{0,T}^2 + \delta_2 \sum_{T \in \mathcal{T}_h} \frac{h_T^2}{\mu_f \alpha \omega} \|\nabla q^h\|_{0,T}^2, \end{aligned}$$

and then  $\vec{\mathbf{v}}^h = \mathbf{0}$ ,  $q^h = 0$  and  $\mathbb{R}(\vec{\mathbf{v}}^h, \xi^h) = 0$ , and in consequence  $\xi^h = 0$ .

□

To conclude this section, the following result establishes the existence and uniqueness of the solution for the discrete problem.

**Theorem 20** (Well-posedness of the discrete problem). *There exists  $h_0 > 0$  such that for all  $h > h_0$  the discrete problem (50) has unique solution  $\vec{\mathbf{u}}^{h*} \in \mathcal{U}_h$ . Moreover, there exists a positive constant  $C_4$  independent of  $h$  such that*

$$\|\vec{\mathbf{u}}^{h*}\|_{\mathcal{U}_h} \leq C_4 \|\mathcal{F}\|_{\mathcal{U}_h} \leq C_4 \left( \|g^p\|_{0,\Gamma_u} + \|\mathbf{g}_{re}\|_{0,\Gamma_p} \right). \quad (61)$$

or equivalently, there exists a positive constant  $\beta_3 > 0$  such that

$$\beta_3 \|\vec{\mathbf{u}}^h\|_{\mathcal{U}_h} \leq \sup_{\substack{\vec{\mathbf{v}}^h \in \mathcal{U}_h \\ \vec{\mathbf{v}}^h \neq \mathbf{0}}} \frac{\langle \mathcal{A}_h(\vec{\mathbf{u}}^h), \vec{\mathbf{v}}^h \rangle}{\|\vec{\mathbf{v}}^h\|_{\mathcal{U}_h}}. \quad (62)$$

*Proof.* The proof follows from the application of Lemmas (12), (18) and (19) plus the Fredholm alternative.  $\square$

### 4.3 Convergence

This section is dedicated to the convergence properties of the method. To this purpose, we assume additional regularity of the solution, i.e., considering the space

$$\mathbf{W} = H^{k+1}(\Omega)^d \times H^{k+1}(\Omega) \times H^k(\Omega),$$

where  $k$  is the order of the finite element spaces (47), and the Lagrange interpolation operators

$$\begin{aligned} \mathcal{I}_H^h &: \mathbf{H} \cap H^{r+1}(\Omega)^d \rightarrow \mathbf{H}_h \\ \mathcal{I}_P^h &: P \cap H^{r+1}(\Omega) \rightarrow P_h \\ \mathcal{I}_S^h &: S \cap H^r(\Omega) \rightarrow S_h. \end{aligned} \quad (63)$$

Then, there exists a constant  $C_{La} > 0$  such that,

$$\begin{aligned} \|\mathbf{v} - \mathcal{I}_H^h \mathbf{v}\|_0 + h \|\mathbf{v} - \mathcal{I}_H^h \mathbf{v}\|_1 &\leq C_{La} h^{k+1} |\mathbf{v}|_{k+1}, \quad \forall \mathbf{v} \in \mathbf{H} \cap H^{r+1}(\Omega)^d \\ \|q - \mathcal{I}_P^h q\|_0 + h \|q - \mathcal{I}_P^h q\|_1 &\leq C_{La} h^{k+1} |q|_{k+1}, \quad \forall q \in P \cap H^{r+1}(\Omega) \\ \|\xi - \mathcal{I}_S^h \xi\|_0 &\leq C_{La} h^k |\xi|_k, \quad \forall \xi \in S \cap H^r(\Omega), \end{aligned} \quad (64)$$

for all  $1 \leq k \leq r$  (see, e.g., [14, Theorem 1.103]). Let us also define  $\mathcal{I}^h := (\mathcal{I}_H^h, \mathcal{I}_P^h, \mathcal{I}_S^h)$ .

The next result concerns the theoretical rate of convergence for the Galerkin scheme (19).

**Theorem 21.** [Convergence] Let  $\vec{\mathbf{u}}$  and  $\vec{\mathbf{u}}^h$  be the solutions of (19) and (50) respectively. In addition, assume that  $\vec{\mathbf{u}} \in \mathbf{U} \cap \mathbf{W}$ . Then, for  $1 \leq k \leq r$ , there exist two constants  $C_1, C_2 > 0$ , independent of  $h$ , such that,

$$\|\vec{\mathbf{u}} - \vec{\mathbf{u}}^h\|_{\mathbf{U}} \leq C_1 h^k \left( \|\mathbf{u}\|_{k+1} + \|p\|_{k+1} + \|\phi\|_k \right) + C_2 \delta_2 h^2 \|\nabla p\|_0 \quad (65)$$

*Proof.* Hereafter, for  $(\mathbf{u}, p, \phi) \in (\mathbf{H}, P, S)$  and for  $(\mathbf{u}^h, p^h, \phi^h) \in (\mathbf{H}_h, P_h, S_h)$ , let us introduce the notations

$$E(\vec{\mathbf{u}}) := \vec{\mathbf{u}} - \mathcal{I}^h \vec{\mathbf{u}} = (\mathbf{u} - \mathcal{I}_H^h \mathbf{u}, p - \mathcal{I}_P^h p, \phi - \mathcal{I}_S^h \phi)$$

and

$$E_h(\vec{\mathbf{u}}, \vec{\mathbf{u}}^h) := \vec{\mathbf{u}}^h - \mathcal{I}^h \vec{\mathbf{u}} = (\mathbf{u}^h - \mathcal{I}_H^h \mathbf{u}, p^h - \mathcal{I}_P^h p, \phi^h - \mathcal{I}_S^h \phi).$$

Let  $\vec{\mathbf{v}}^h \in \mathbf{U}_h$ . Using Lemma (20) and Lemma (16) we obtain

$$\begin{aligned} \beta_3 \|E_h(\vec{\mathbf{u}}, \vec{\mathbf{u}}^h)\| &\leq \sup_{\substack{\vec{\mathbf{v}}^h \in \mathbf{U}_h \\ \vec{\mathbf{v}}^h \neq \vec{\mathbf{0}}} } \frac{|\langle \mathcal{A}_h(E_h(\vec{\mathbf{u}}, \vec{\mathbf{u}}^h)), \vec{\mathbf{v}}^h \rangle|}{\|\vec{\mathbf{v}}^h\|_{\mathbf{U}_h}} \\ &\leq \sup_{\substack{\vec{\mathbf{v}}^h \in \mathbf{U}_h \\ \vec{\mathbf{v}}^h \neq \vec{\mathbf{0}}} } \frac{\left| \langle \mathcal{A}_h(E(\vec{\mathbf{u}})), \vec{\mathbf{v}}^h \rangle - \delta_2 \sum_{T \in \mathcal{T}_h} \frac{h_T^2}{\mu_f \alpha \omega} (\nabla p, \nabla q^h)_T \right|}{\|\vec{\mathbf{v}}^h\|_{\mathbf{U}_h}}. \end{aligned}$$

Utilizing the continuity of  $\mathcal{A}_h$  (inequality (58)) we get

$$|\langle \mathcal{A}_h(E(\vec{\mathbf{u}})), \vec{\mathbf{v}}^h \rangle| \leq \eta_4 \|E(\vec{\mathbf{u}})\|_{\mathcal{U}} \|\vec{\mathbf{v}}^h\|_{\mathcal{U}_h} \leq C_{\text{La}} h^k \left( |\mathbf{u}|_{k+1} + |p|_{k+1} + |\phi|_k \right) \|\vec{\mathbf{v}}^h\|_{\mathcal{U}_h}.$$

In addition, it holds

$$\begin{aligned} \left| \delta_2 \sum_{T \in \mathcal{T}_h} \frac{h_T^2}{\mu_f \alpha \omega} (\nabla p, \nabla q^h)_T \right| &\leq h^2 \delta_2 \frac{1}{\mu_f \alpha \omega} \left( \sum_{T \in \mathcal{T}_h} \|\nabla p\|_{0,T}^2 \right)^{1/2} \left( \sum_{T \in \mathcal{T}_h} \|\nabla q^h\|_{0,T}^2 \right)^{1/2} \\ &= \delta_2 \left( \frac{h^2}{\kappa} \right) \|\nabla p\|_0 \left( \frac{\kappa}{\mu_f \alpha \omega} \right)^{\frac{1}{2}} \|\vec{\mathbf{v}}^h\|_{\mathcal{U}_h} \end{aligned} \quad (66)$$

with  $\tilde{C}_2 = (\mu_f \alpha \kappa)^{-\frac{1}{2}}$ , which allows to conclude

$$\|E_h(\vec{\mathbf{u}}, \vec{\mathbf{u}}^h)\| \leq \beta_3^{-1} C_{\text{La}} h^k \left( |\mathbf{u}|_{k+1} + |p|_{k+1} + |\phi|_k \right) + \beta_3^{-1} \tilde{C}_2 \delta_2 h^2 \|\nabla p\|_0.$$

Applying the triangle inequality and using (64) yields

$$\begin{aligned} \|\vec{\mathbf{u}} - \vec{\mathbf{u}}^h\|_{\mathcal{U}_h} &\leq \|E(\vec{\mathbf{u}})\|_{\mathcal{U}_h} + \|E_h(\vec{\mathbf{u}}, \vec{\mathbf{u}}^h)\|_{\mathcal{U}_h} \\ &\leq (1 + \beta_3^{-1}) C_{\text{La}} h^k \left( |\mathbf{u}|_{k+1} + |p|_{k+1} + |\phi|_k \right) + \beta_3^{-1} \tilde{C}_2 \delta_2 h^2 \|\nabla p\|_0 \end{aligned}$$

concluding the proof.  $\square$

## 5 Numerical Examples

This section is devoted to the numerical results. The first three examples aim at validating the method and the theoretical expectations presented in Section 6. For these purposes, we introduce some analytical solutions. Since every solution  $v$  is a complex function, they are written as  $v = (\text{Re } v \text{ Im } v)$ . Additional examples will address the robustness of the solver in layered domains as well as its application in a realistic setting using a brain geometry segmented from magnetic resonance medical images.

Concerning the computational aspect, the software MAD ([17], chapter 5) is used for the finite element framework, based upon the linear algebra library PETSc [3]. The inversion of the system of equations is done by means of the MUltifrontal Massively Parallel sparse direct Solver (MUMPS, [2]).

### 5.1 Example 1: Validation against an analytical solution

We first validate the numerical method in a case in which the problem (4) can be solved analytically, and whose solution is given by,

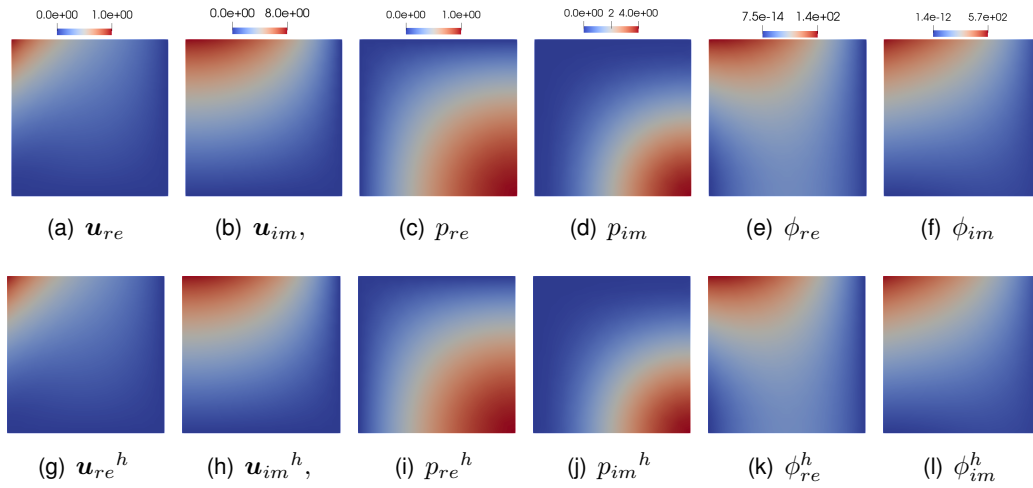


Figure 1: Example 1 (2D): Analytical solution (top) and numerical results of (4) for  $h = 0.0625$ . The parameters in (49) are set to  $\delta_1 = 0.5$  and  $\delta_2 = 0$ , due to the comparatively high value of  $\kappa$  (see Table 1).

$$\begin{aligned}
 \mathbf{u} &= (\operatorname{Re} \mathbf{u} \quad \operatorname{Im} \mathbf{u}) = \begin{pmatrix} (x-1)^2 y^2 & (x-1)(x+2)^2 y(y+1) \\ xy(x-1) & 2x^2 y(x-1) \end{pmatrix} \\
 p &= (\operatorname{Re} p \quad \operatorname{Im} p) = \left( \sin\left(\frac{\pi x}{2}\right) \cos\left(\frac{\pi y}{2}\right) \quad (1 - \cos(\pi x))(1 + \cos(\pi y)) \right) \\
 \phi &= (\operatorname{Re} \phi \quad \operatorname{Im} \phi) \\
 &= \left( \sin\left(\frac{\pi x}{2}\right) \cos\left(\frac{\pi y}{2}\right) - \lambda \operatorname{tr}(\varepsilon(\operatorname{Re} \mathbf{u})) \quad (1 - \cos(\pi x))(1 + \cos(\pi y)) - \lambda \operatorname{tr}(\varepsilon(\operatorname{Im} \mathbf{u})) \right)
 \end{aligned} \tag{67}$$

for 2D on the unit square and,

$$\begin{aligned}
 \mathbf{u} &= (\operatorname{Re} \mathbf{u} \quad \operatorname{Im} \mathbf{u}) = \begin{pmatrix} (x-1)^2 xy^2(z+2) & (x-1)x^2 y^2(z+1) \\ x^3 y(z+1)^2(x-1)^3 & (x-1)^2 x^3 y^3(z-2) \\ (x-1)xy(z+2)^2 & x^2 y(x-1)(z-2)^2 \end{pmatrix} \\
 p &= (\operatorname{Re} p \quad \operatorname{Im} p) = \left( \sin\left(\frac{\pi x}{2}\right) \cos\left(\frac{\pi y}{2}\right) \quad (1 - \cos(\pi x))(1 + \cos(\pi y)) \right) \\
 \phi &= (\operatorname{Re} \phi \quad \operatorname{Im} \phi) \\
 &= \left( \cos\left(\frac{\pi y}{2}\right) \sin(\pi z) - \lambda \operatorname{tr} \varepsilon(\operatorname{Re} \mathbf{u}) \quad \sin\left(\frac{\pi z}{2}\right) (1 + \cos(\pi y))(1 + \cos(\pi z)) - \lambda \operatorname{tr} \varepsilon(\operatorname{Im} \mathbf{u}) \right)
 \end{aligned} \tag{68}$$

for 3D on the unit cube, respectively.

Boundary conditions are prescribed according to the exact solutions (67) and (68), evaluated on the sets:

$$\Gamma_p^{2D} = \{(x, y) \in \mathbb{R}^2 : x = 0, y = 1\},$$

and,

$$\Gamma_u^{2D} = \{(x, y) \in \mathbb{R}^2 : x = 1, y = 0\},$$

for pressure and velocity in 2D (resp.), and on,

$$\Gamma_p^{3D} = \{(x, y, z) \in \mathbb{R}^3 : x = 0, x = 1, y = 0\},$$

and,

$$\Gamma_u^{3D} = \{(x, y, z) \in \mathbb{R}^3 : y = 1, z = 0, z = 1\},$$

for pressure and velocity in 3D, respectively.

The set of physical parameters for both 2D and 3D simulations, is described in table (1).

Parameter	$E$ [dyn/cm <sup>2</sup> ]	$\nu$	$\mu_f$ [Poise]	$\kappa$ [cm <sup>4</sup> ]	$\omega$	$\rho$ [gr/cm <sup>3</sup> ]
Value	$10^2$	0.4	1.0	0.1	1.0	1.0

Table 1: Parameters used for the examples with analytical solutions.

The computational domain is based on several refinements of a unstructured triangular/tetrahedron mesh (coarsest discretization  $h = 1$  mm). The 2D numerical solutions for this example are shown in Figure 1, together with the exact solutions (67).

Figure 2 shows the error with respect to the exact solution for displacement, pressure, and total pressure, as a function of the mesh size, setting  $\delta_1 = 0.5$  and  $\delta_2 = 0.0$ . The convergence rates confirm the theoretical expectations discussed in Section 4 both for linear and quadratic finite elements.

We can draw the same conclusion for the three-dimensional case by inspection of the convergence results in Figure 3.

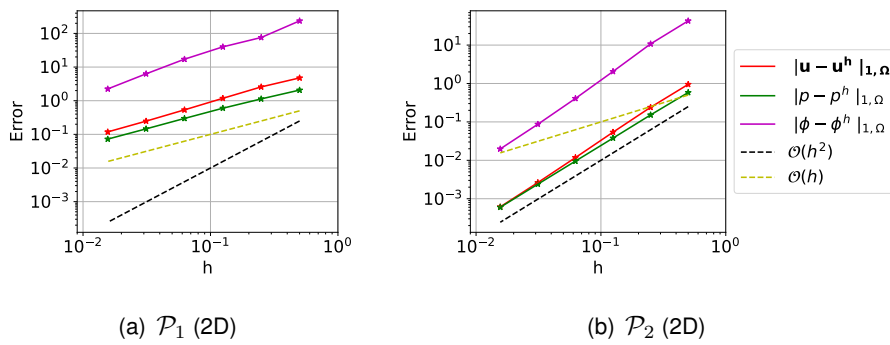


Figure 2: Example 1 (2D). Error for displacement, pressure, and total pressure as a function of the mesh size, for linear (left) and quadratic (right) finite elements.

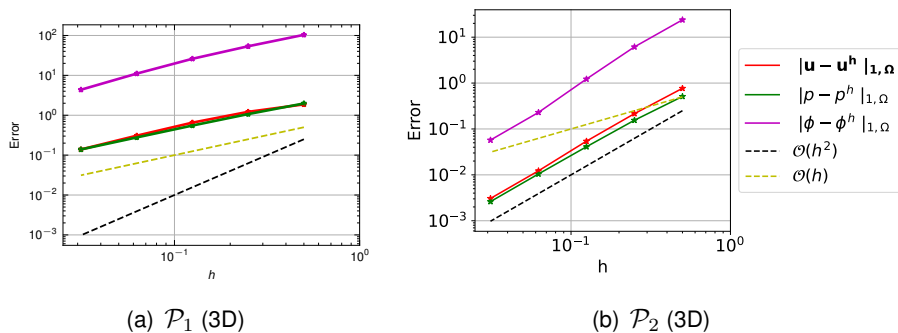


Figure 3: Example 1 (3D). Error for displacement, pressure, and total pressure as a function of the mesh size, for linear (left) and quadratic (right) finite elements.

To demonstrate the relevance of the Brezzi-Pitkäranta stabilization term for low permeabilities, Figure 4 shows the numerical error for three different mesh sizes and a wide range of permeabilities. c The

stabilized version ( $\delta_2 = 1$ ) leads to a very robust solver with an error independent on the permeability. This is in contrast with the  $\delta_2 = 0$  case, where the error significantly increases in the low permeability range.

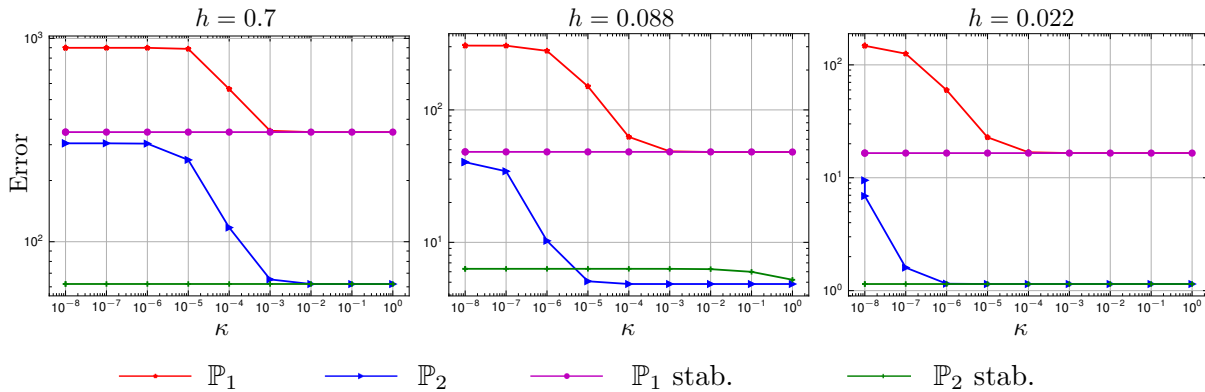


Figure 4: Example 1 (2D): Numerical error as a function of the permeability parameter  $\kappa$  for different mesh sizes, comparing the case  $\delta_2 = 0$  (red and blue curves) with the stabilized version  $\delta_2 = 1$  (magenta and green curves).

## 5.2 Example 2: Layered domain

In this section we considered a two-dimensional domain containing layers with different permeabilities. The purpose of this example is to validate the robustness of the numerical solutions, in particular of the pressure, in presence of discontinuous coefficients, spanning different orders of magnitude. Addressing such problems is relevant in different fields of applications, including soil mechanics and biomedical engineering, particularly in scenarios where the system parameters are affected by uncertainty and/or have to be estimated.

We set  $\Omega = [0, 1] \times [0, 1]$ , decomposed in three subdomains with  $\kappa_1 = 10^{-3} \text{ cm}^4$  for  $y \in [0, 1/3]$ ,  $\kappa_2 = 10^{-4} \text{ cm}^4$ , for  $y \in [1/3, 2/3]$  and  $\kappa_3 = 10^{-5} \text{ cm}^4$  for  $y \in [2/3, 1]$ . (see Figure 5). The values of the other physical parameters are provided in Table 2.

Parameter	$E$ [dyn/cm <sup>2</sup> ]	$\nu$	$\mu_f$ [Poise]	$\kappa$ [cm <sup>2</sup> ]	$\omega$ [Hz]	$\rho$ [gr/cm <sup>3</sup> ]
Value	$10^2$	0.45	$10^{-2}$	$10^{-3} \mid 10^{-4} \mid 10^{-5}$	25   50   75   100   125	1.0

Table 2: Parameters used for the Example (5.2) with different permeabilities.

Concerning the boundary conditions, we set a Neumann boundary condition on the square bottom of magnitude  $10^{-2} \text{ dyn/cm}^2$  pointing upwards, zero displacements at the top of the geometry, and a constant pressure field at the bottom of  $10^{-2} \text{ dyn/cm}^2$ .

We consider an unstructured triangular mesh with characteristic size of  $h = 4 \times 10^{-3} \text{ cm}$ , and stabilization parameters  $\delta_1 = \omega^{-2}$  (inf-sup stabilization) and  $\delta_2 = 1$  (pressure stabilization).

The magnitude of the solutions obtained for different values of  $\omega$  are shown in Figures 6, for displacement and total pressure. The solutions for the pressure are analyzed in more detail in Figure 7, highlighting that the numerical solution is not affected by the discontinuities and by the small values of the permeability.

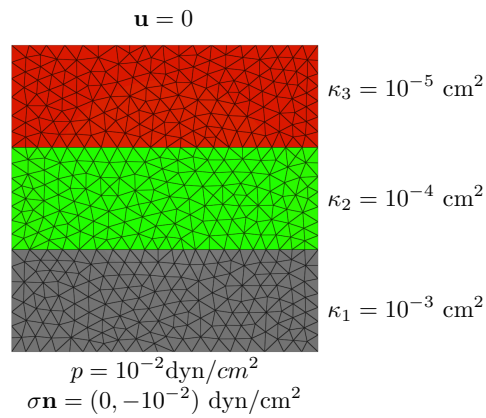


Figure 5: Example 3 (layered domain): Set-up of the computational domain with varying permeability (on a coarse mesh).

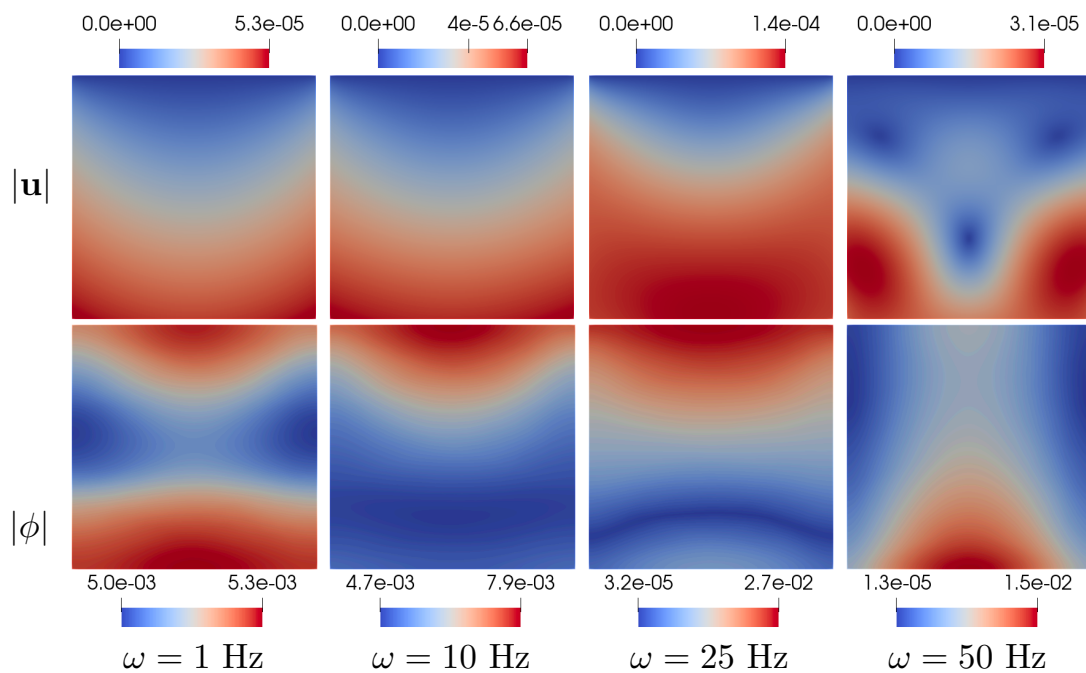


Figure 6: Example 3 (layered domain): Magnitudes of the displacement and total pressure solutions for different excitation frequencies. The stabilization parameters in (49) are set to  $\delta_1 = \omega^{-2}$  and  $\delta_2 = 1.0$

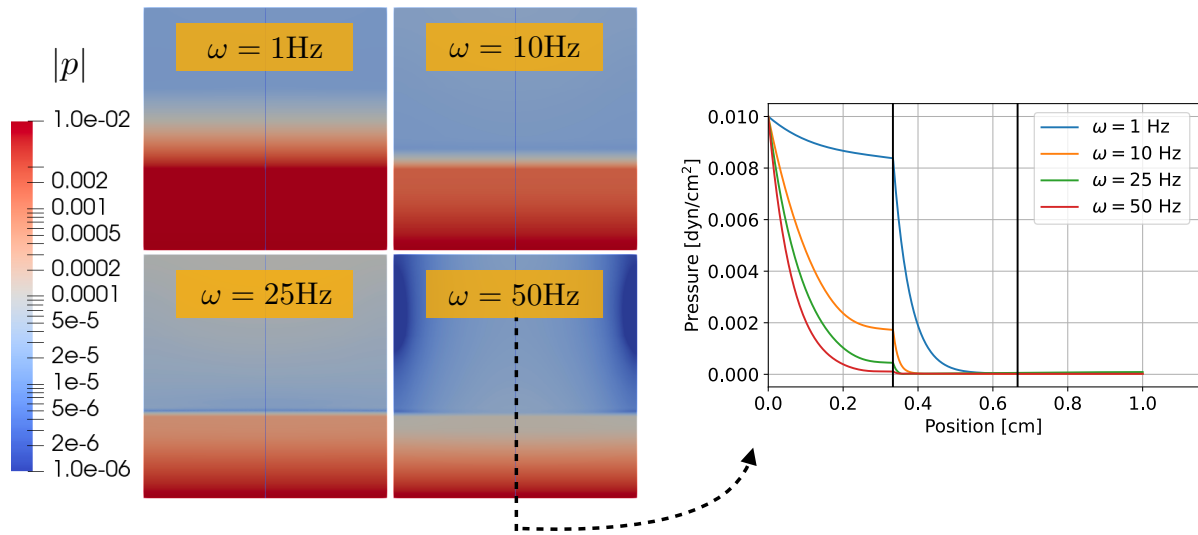


Figure 7: Example 3 (layered domain): Pressure profiles at vertical control line. The solver shows a robust behavior against discontinuities in the permeability field. The permeability interfaces are indicated with black lines in the right plot.

Although an exact solution for this benchmark is not available, One can further infer the validity of the results in terms of the expected elastic behavior of the wave within the media. The parameter set of the simulations impose a wave speed  $\sqrt{E/\rho} = 10$  cm/s, leading to wavelengths of approximately 62 cm, 6.28 cm, 2.51 cm, 1.27 cm for frequencies of 1 Hz, 10Hz, 25 Hz and 50 Hz, respectively. This explains why in the low frequency simulation the domain size (1 cm) does not allow a full wave cycle to develop, whereas an almost full wavelength is depicted for  $\omega = 50Hz$ .

### 5.3 Example 3: Three-dimensional brain geometry

The final test case considers the simulation of a magnetic resonance elastography (MRE) experiment on a realistic brain geometry obtained from medical imaging. The computational mesh geometry is depicted in Figure 8. The boundaries of the domain are decomposed in disjoint sets  $\partial\Omega = \Gamma_{\text{neck}} \cup \Gamma_{\text{MRE}} \cup \Gamma_{\text{ventricles}}$ , and we prescribe the following boundary conditions:

- MRE pulse:  $\sigma \mathbf{n} = [0, 10^3, 0]$  on  $\Gamma_{\text{MRE}}$ .
- Fixed sub-domain:  $\text{Re } \mathbf{u} = \text{Im } \mathbf{u} = 0$  on  $\Gamma_{\text{neck}}$ .
- Intracranial pressure:  $\text{Re } p = 10^4$  dyn/cm<sup>2</sup> on  $\partial\Omega \setminus \Gamma_{\text{ventricles}}$ .
- Pathological ventricle pressure:  $\text{Re } p = 1.1 \times 10^4$  dyn/cm<sup>2</sup> on  $\Gamma_{\text{ventricles}}$ .
- $\text{Im } p = 0$  on  $\partial\Omega$ .

Parameter	$E$	$\nu$	$\mu_f$	$\kappa$	$\omega$	$\rho$
Value	$10^6$ [dyn/cm <sup>2</sup> ]	0.4	0.01 [Poise]	$10^{-8}$ [cm <sup>2</sup> ]	10.0 [Hz]	1.0 [gr/cm <sup>3</sup> ]

Table 3: Parameter set for human brain simulation.

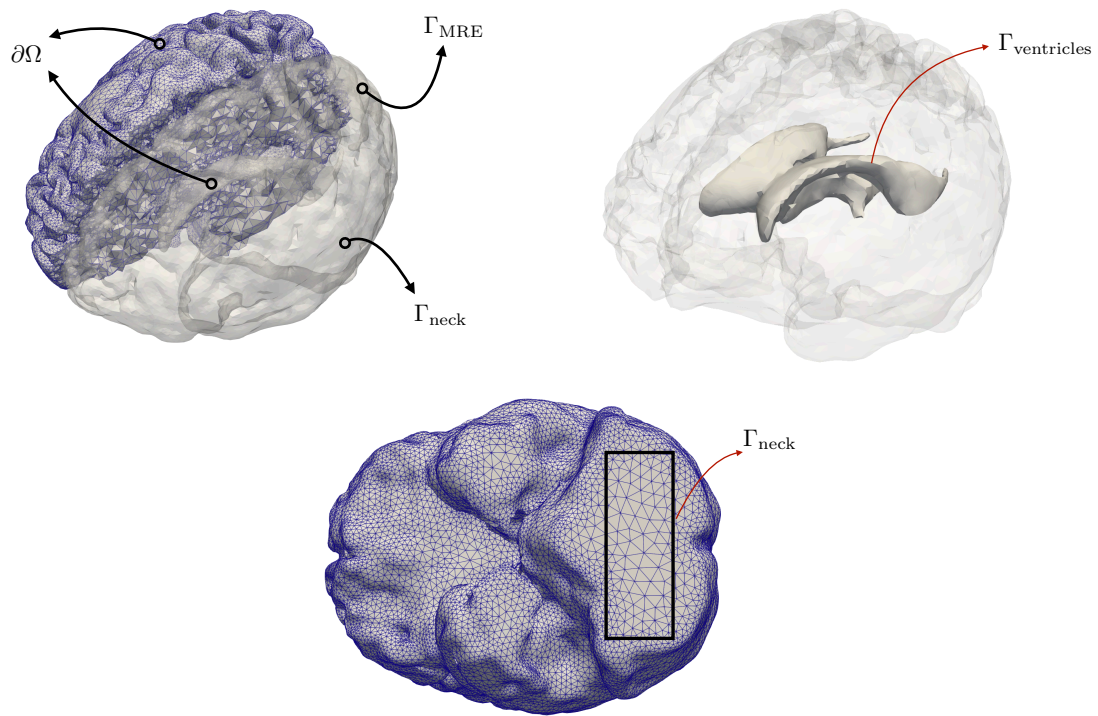


Figure 8: Example 4 (brain elastography): Computational domain (Source: [16])

The intensity of the MRE pulse boundary condition is chosen to get physiological magnitudes for the displacement fields. An intracranial pressure difference is imposed between the ventricles and the exterior boundary, emulating pathological conditions.

The physical parameters are chosen to mimic the setting presented in [16] (see Table 3). To handle the low permeability value, the Brezzi-Pitkäranta stabilization term with  $\delta_2 = 1$  is considered.

The computational tetrahedral mesh has been generated from the segmented surface mesh using the software MMG [12], and it is composed of 103k vertices and 511k tetrahedra. Employing a linear equal-order interpolation for the unknowns leads to a problem with 516k degrees of freedom.

The numerical results with this configuration are depicted in figure 9.

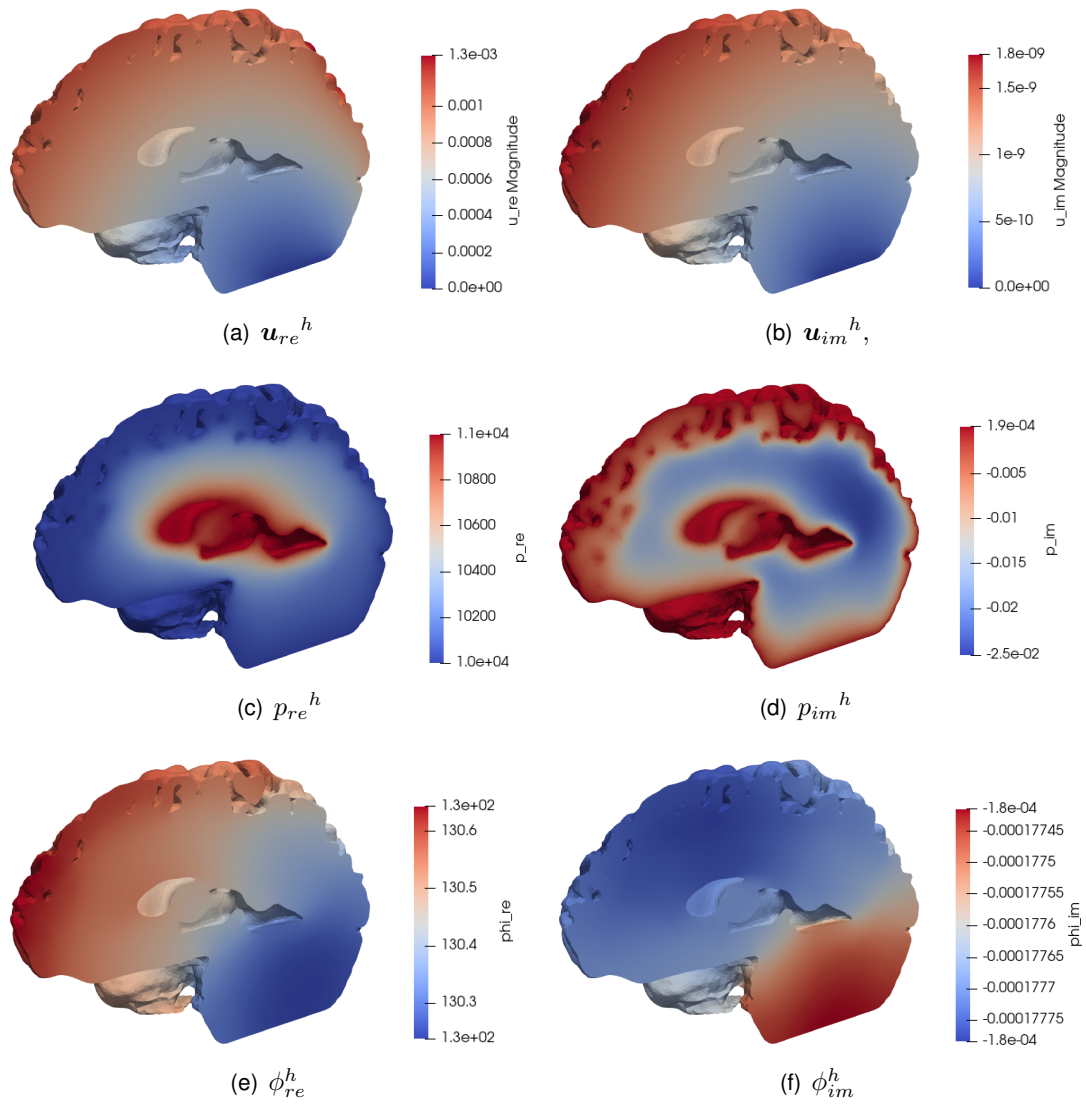


Figure 9: Example 4 (brain elastography): Numerical results for displacement (top row), pressure (middle row) and total pressure (bottom row).

## 6 Conclusions

This paper proposes and analyzes a stabilized finite element method for the numerical solution of the Biot equations in the frequency domain utilizing a total-pressure formulation. We focus on the case of equal-order finite elements, introducing additional stabilization terms to cure numerical instabilities. Moreover, an additional Brezzi-Pitkäranta stabilization is introduced to enhance robustness concerning the discontinuities of material permeability.

The first contribution of this work is the detailed numerical analysis, in the continuous and the discrete settings, of the total pressure formulation. In particular, using the Fredholm alternative [15, 38], and the T-coercivity properties of the variational form [10], we show that the well-posedness results of [28] in the time domain case can be extended to the frequency regime. The second contribution concerns the proposed stabilization, which allows to enhancement of the robustness of the numerical method in a wide range of tissue permeability and also in the presence of discontinuities.

Since the additional stabilization introduces a second-order consistency error, optimal convergence can be proven only for linear equal-order finite elements. However, in practical situations, it is important to observe that the stabilization can be introduced only where required (i.e., regions of very low permeability), thus expecting numerical results of better quality than those suggested by the theoretical expectation. An optimal choice of the stabilization parameters depending on the local solutions or considering local error estimators is the subject of ongoing research and is out of the scope of this work.

The proposed method has been validated on simple examples against analytical solutions, as well as considering a layered domain with varying permeability, and an example of a brain geometry obtained from medical imaging. Future directions of this research will consider the application of the scheme in the context of inverse problems for parameters or state estimation.

## Acknowledgments

This research is funded by the Deutsche Forschungsgemeinschaft (DFG, German Research Foundation) under Germany's Excellence Strategy - MATH+: The Berlin Mathematics Research Center [EXC-2046/1 - project ID: 390685689]. The second author would like to acknowledge the financial support from the project DI VINCI PUCV 039.331/2023, and the support of the student Mauricio Portilla concerning a few advances on the software used for the numerical experiments within this work.

## References

- [1] E. Ahmed, F. Radu, and J. Nordbotten. Adaptive poromechanics computations based on a posteriori error estimates for fully mixed formulations of biot's consolidation model. *Computer Methods in Applied Mechanics and Engineering*, 347:264–294, 2019.
- [2] P.R. Amestoy, I. S. Duff, J. Koster, and J.-Y. L'Excellent. A fully asynchronous multifrontal solver using distributed dynamic scheduling. *SIAM Journal on Matrix Analysis and Applications*, 23(1):15–41, 2001.

- [3] S. Balay, S. Abhyankar, Adams. M.D., J. Brown, P. Brune, K. Buschelman, L. Dalcin, V. Eijkhout, W.D. Gropp, D. Kaushik, M.G. Knepley, L.C. McInnes, K. Rupp, B.F. Smith, S. Zampini, and H. Zhang. PETSc Web page, 2015.
- [4] F. Bertrand, M. Brodbeck, and T. Ricken. On robust discretization methods for poroelastic problems: Numerical examples and counter-examples. *Examples and Counterexamples*, 2:100087, 2022.
- [5] M. Biot. General theory of three-dimensional consolidation. *Journal of Applied Physics*, 12:155–164, 1941.
- [6] D. Boffi, M. Botti, and D. A. Di Pietro. A nonconforming high-order method for the biot problem on general meshes. *SIAM Journal on Scientific Computing*, 38(3):A1508–A1537, 2016.
- [7] S. C. Brenner and L. R. Scott. *The Mathematical Theory of Finite Element Methods*. Springer New York, NY, New York, 2007.
- [8] F. Brezzi and J. Pitkäranta. On the stabilization of finite element approximations of the stokes equations. In Wolfgang Hackbusch, editor, *Efficient Solutions of Elliptic Systems*, volume 10 of *Notes on Numerical Fluid Mechanics*. Vieweg+Teubner Verlag, Wiesbaden, 1984.
- [9] R. Bürger, S. Kumar, D. Mora, R. Ruiz-Baier, and N. Verma. Virtual element methods for the three-field formulation of time-dependent linear poroelasticity. *Advances in Computational Mathematics*, 47(1):2, 2021.
- [10] P. Ciarlet. T-coercivity: Application to the discretization of helmholtz-like problems. *Computers & Mathematics with Applications*, 64:22–34, 2012.
- [11] P. G. Ciarlet. *Linear and nonlinear functional analysis with applications : with 401 problems and 52 figures*. Society for Industrial and Applied Mathematics, 3600 University City Science Center, Philadelphia, PA, United States, October 9 2013.
- [12] C. Dapogny, C. Dobrzynski, and P. Frey. Three-dimensional adaptive domain remeshing, implicit domain meshing, and applications to free and moving boundary problems. *J. Comp. Phys.*, 262:358—378, 2014.
- [13] E. Eliseussen, M.E. Rognes, and T.B. Thompson. A posteriori error estimation and adaptivity for multiple-network poroelasticity. *ESAIM: M2AN*, 57(4):1921–1952, 2023.
- [14] A. Ern and L. Guermond. *Theory and Practice of Finite Elements*. Springer Verlag New York, NY, New York, 2004.
- [15] Lawrence C. Evans. *Partial Differential Equations*. American Mathematical Society, 2010.
- [16] F. Galarce, K. Tabelow, J. Polzehl, C.P. Panagiotis, V. Vavourakis, L. Lilaj, I. Sack, and A. Caiazzo. Displacement and pressure reconstruction from magnetic resonance elastography images: Application to an in silico brain model. *SIAM Journal on Imaging Science*, 2023.
- [17] F. Galarce Marin. *Inverse problems in hemodynamics. Fast estimation of blood flows from medical data*. PhD thesis, INRIA Paris & Laboratoire Jacques-Louis Lions. Sorbonne Université, 2021.
- [18] G.N. Gatica, N. Heuer, and S. Meddahi. On the numerical analysis of nonlinear twofold saddle point problems. *IMA Journal of Numerical Analysis*, 23(2):301–330, 2003.

- [19] G.N. Gatica, R. Oyarzúa, and F. Sayas. Analysis of fully-mixed finite element methods for the stokes–darcy coupled problem. *Math. Comp.*, 80:1911–1948, 2011.
- [20] V. Girault and P.-A. Raviart. *Finite Element Approximation of the Navier-Stokes Equations*. Springer Berlin, Heidelberg, New York, 1979.
- [21] S. Hirsch, J. Braun, and I. Sack. *Magnetic Resonance Elastography: Physical Background And Medical Applications*. Wiley, 2017.
- [22] A. Khan and D.J. Silvester. Robust a posteriori error estimation for mixed finite element approximation of linear poroelasticity. *IMA Journal of Numerical Analysis*, 41(3):2000–2025, 10 2020.
- [23] R. Kress. Fredholm’s alternative for compact bilinear forms in reflexive banach spaces. *Journal of Differential Equations*, 25:216–226, 1977.
- [24] J. J. Lee. Robust error analysis of coupled mixed methods for biot’s consolidation model. *Journal of Scientific Computing*, 69(2):610–632, 2016.
- [25] Y. Li and L. T. Zikatanov. Residual-based a posteriori error estimates of mixed methods for a three-field Biot’s consolidation model. *IMA Journal of Numerical Analysis*, 42(1):620–648, 10 2020.
- [26] H. Mella, E. Sáez, and J. Mura. A hybrid pml formulation for the 2d three-field dynamic poroelastic equations. *Computer Methods in Applied Mechanics and Engineering*, 2023. To appear in *Computer Methods in Applied Mechanics and Engineering*, 2023.
- [27] M.A. Murad and A.F.D. Loula. Improved accuracy in finite element analysis of biot’s consolidation problem. *Computer Methods in Applied Mechanics and Engineering*, 95(3):359–382, 1992.
- [28] R. Oyarzúa and R. Ruiz-Baier. Locking-free finite element methods for poroelasticity. *SIAM J. Numer. Anal.*, 54(5):2951–2973, 2016.
- [29] P. R. Perriñez, F. E. Kennedy, E. E. Van Houten, J. B. Weaver, and K. D. Paulsen. Magnetic resonance poroelastography: an algorithm for estimating the mechanical properties of fluid-saturated soft tissues. *IEEE Transactions on Medical Imaging*, 29(3):746–755, 2010.
- [30] P. J. Phillips and M. F. Wheeler. A coupling of mixed and discontinuous galerkin finite-element methods for poroelasticity. *Computational Geosciences*, 12(4):417–435, 2008.
- [31] P. Joseph Phillips and M. F. Wheeler. Overcoming the problem of locking in linear elasticity and poroelasticity: An heuristic approach. *Computational Geosciences*, 13:5–12, January 2009.
- [32] M. Renardy and R.C. Rogers. *An Introduction to Partial Differential Equations*. Texts in Applied Mathematics. Springer New York, NY, 2 edition, 2004.
- [33] R. Riedlbeck, D. A. Di Pietro, A. Ern, S. Granet, and K. Kazymyrenko. Stress and flux reconstruction in biot’s poro-elasticity problem with application to a posteriori error analysis. *Computers & Mathematics with Applications*, 73(7):1593–1610, 2017.
- [34] I. Sack. Magnetic resonance elastography from fundamental soft-tissue mechanics to diagnostic imaging. *Nat. Rev. Phys.*, 5:25–42, 2023.
- [35] R.E. Showalter. Diffusion in poro-elastic media. *Journal of Mathematical Analysis and Applications*, 251(1):310–340, 2000.

- [36] S. P. Sourbron and D. L. Buckley. Tracer kinetic modelling in mri: estimating perfusion and capillary permeability. *Physics in Medicine & Biology*, 57(2):R1, dec 2011.
- [37] D. R. Sowinski, M.D.J. McGarry, E. E. W. Van Houten, S. Gordon-Wylie, J. B. Weaver, and K. D. Paulsen. Poroelasticity as a Model of Soft Tissue Structure: Hydraulic Permeability Reconstruction for Magnetic Resonance Elastography in Silico. *Frontiers in Physics*, 8:617582, 2020.
- [38] O. Steinbach. *Numerical Approximation Methods for Elliptic Boundary Value Problems*. Springer New York, NY, New York, 2007.
- [39] L. Tan, M. D. J. McGarry, E. W. Van Houten, M. Ji, L. Solamen, W. Zeng, J.B. Weaver, and K. D. Paulsen. A numerical framework for interstitial fluid pressure imaging in poroelastic MRE. *PLOS ONE*, 12(6):1–22, 06 2017.
- [40] A.-T. Vuong. *A Computational Approach to Coupled Poroelastic Media Problems*. PhD thesis, Technische Universität München, 2016.
- [41] J. Wang, M. Fernández-Seara, S. Wang, and K. Lawrence. When perfusion meets diffusion: in vivo measurement of water permeability in human brain. *Journal of Cerebral Blood Flow & Metabolism*, 27(4):839–849, 2007.
- [42] S.-Y. Yi. Convergence analysis of a new mixed finite element method for biot's consolidation model. *Numerical Methods for Partial Differential Equations*, 30(4):1189–1210, 2014.
- [43] L. Zhang, L. Scholtès, and F. V. Donzé. Discrete element modeling of permeability evolution during progressive failure of a low-permeable rock under triaxial compression. *Rock Mechanics and Rock Engineering*, 54:6351–6372, 2021.